

Simulations of tidal disruption events for *eROSITA*

Bachelorarbeit aus der Physik

Vorgelegt von
Melanie Lang
27. September 2017

Dr. Karl Remeis Sternwarte Bamberg
Friedrich-Alexander-Universität Erlangen-Nürnberg



Betreuer: Prof. Dr. Jörn Wilms

Abstract

The aim of this thesis is to investigate the detectability of tidal disruption events (TDEs) by *eROSITA*. *eROSITA* is a X-ray telescope and will perform the next all-sky survey in the X-ray regime. Therefore, it is well suited to discover many TDEs, a not well understood kind of sources until now. The discovery of new TDEs is with pointed observations only possible by accident. Due to this fact, it is expected that *eROSITA* will bring development in discovering new TDEs. After giving some information on the *eROSITA* mission, I present the so far accepted theoretical background of tidal disruption events. To get some further basic knowledge, two spectra of known TDEs are analyzed. Then it is time to turn to the simulation part. Here at first a source catalogue is implemented. For the analysis of the simulated data I concentrate on the lightcurve of one TDE. The ability to identify it within one all-sky survey is discussed. On the one hand it is studied for the case that a tidal disruption is caused by a super massive black hole. And on the other hand for the case that it is caused by an intermediate mass black hole. Finally, there are an outlook and suggestions, what could be improved in this work.

Zusammenfassung

Das Ziel dieser Arbeit ist es, die Detektierbarkeit von Ereignissen, bei denen Sterne aufgrund der Gezeitenkräfte von schwarzen Löchern zerissen werden, durch *eROSITA* zu untersuchen. Diese Ereignisse werden “tidal disruption events (TDEs)” genannt. Das Röntgen-Teleskop *eROSITA* wird die nächste, vollständige Untersuchung des Himmels im Röntgenbereich durchführen. Aus diesem Grund ist es gut geeignet, neue TDEs zu entdecken, was bei Beobachtungen eines einzigen Punktes am Himmel nur durch Zufall möglich ist. Diese besondere Sorte von Quellen ist bisher unzureichend verstanden, weshalb *eROSITA* hier Fortschritte bringen könnte. Nach Informationen zur *eROSITA* Mission werde ich den bisher akzeptierten Stand des theoretischen Hintergrunds der TDEs darlegen. Um weitere Grundkenntnisse über diese Ereignisse zu erhalten, werden anschließend zwei Spektren von bekannten TDEs analysiert. Nach dieser Analyse kann sich dem Simulationsteil dieser Arbeit zugewandt werden. Dafür wird zuerst ein Quellkatalog implementiert. Bei der Analyse der simulierten Daten habe ich mich auf die Lichtkurve einer Quelle beschränkt. Es wird erörtert, inwieweit es möglich ist, ein TDE innerhalb eines Scans des gesamten Himmels als ein solches zu identifizieren. Einerseits wird dies für den Fall untersucht, dass ein Stern durch die Gezeitenkräfte eines super massiven schwarzen Lochs zerissen wird. Und andererseits für den Fall, dass die Gezeitenkräfte durch ein schwarzes Loch mit intermediärer Masse hervorgerufen werden. Zu guter Letzt werden noch Verbesserungsvorschläge gegeben und ein Ausblick, was man sich von der *eROSITA* Mission erhoffen kann.

Contents

1	Introduction	6
2	The <i>eROSITA</i> Mission	7
2.1	Technical details	7
2.2	X-ray telescopes and detectors	9
2.2.1	Wolter telescopes	9
2.2.2	X-ray CCDs	9
2.3	All-sky survey and observing strategy	10
3	Theoretical background - TDEs	12
4	Data analysis	18
4.1	NGC 3599	18
4.1.1	Source description	18
4.1.2	Observational details	18
4.1.3	Data reduction	18
4.1.4	Data analysis	19
4.2	<i>Swift</i> J2058.4+0516	21
4.2.1	Source description	21
4.2.2	Observational details	21
4.2.3	Data reduction	23
4.2.4	Data analysis	23
5	The <i>SIXTE</i>-Software	26
5.1	<i>SIXTE</i>	26
5.2	<i>erosim</i>	27
5.3	<i>SIMPUP</i>	27
6	Simulations for <i>eROSITA</i>	29
6.1	Source catalogue	29
6.2	Result of the all-sky survey simulation	31
6.2.1	Results for TDEs by SMBHs	32
6.2.2	Results for TDEs by IMBHs	36
6.3	Conclusions of the simulations	39
7	Conclusions	40
8	Outlook	41
	References	42

Contents	5
Acknowledgment	44
Eigenständigkeitserklärung	45

1 Introduction

Black holes are fascinating many people, not only scientists but laymen as well. Therefore, there is a multitude of books and movies covering this topic. Inside a black hole the gravitational force is so strong that not even light can escape it. Furthermore, it is bending space-time and can swallow a large amount of matter. An example where one can see the great force of black holes are tidal disruption events (TDEs), where a whole star is torn apart by tidal forces. These events are a great chance to probe accretion physics near the event horizon or relativity. Additionally they form another possibility to estimate the spin of a black hole (Komossa, 2012). Several candidate tidal disruption events are known so far, discovered from optical via UV to X-rays (Komossa, 2015). It is difficult to discover a tidal disruption event because the probability to observe one by accident during a pointed observation is low. Therefore, an all-sky survey is well suited for this task. The last all-sky survey in the X-ray band was done by *ROSAT* in 1990/91 (Truemper, 1982). *eROSITA* will do the next one. This time with higher sensitivity. When a TDE is discovered by *eROSITA*, follow-up observations with other telescopes are possible, which will lead to a better understanding of these events.

An interesting question now is, how a TDE looks like when detected by *eROSITA*. This question can only be answered by simulations so far. In return, simulations done now will help to identify a tidal disruption event at the time real data is available. Due to this reason I combined data analysis of known TDEs with simulations for *eROSITA* in my thesis.

The first part of this thesis will give a brief overview of the *eROSITA* mission. Then the theoretical background of TDEs will be provided. After that two data sets are analyzed: one of Swift J2058.4+0516 (hereafter Sw J2058+05) and one of NGC 3599. The data analysis is followed by the simulation part. Here the knowledge about tidal disruption events is applied to simulate those events by using a simulation program suited for the *eROSITA* mission. At first a brief overview of this used software is given before presenting the results of the simulations. So far, many theoretical aspects only consider tidal disruption events by super massive black holes. But TDEs by intermediate mass black holes are even more interesting. The decline in their lightcurves is very fast, which makes it easier to identify them as tidal disruption events. Additionally, they are thought to happen more often than TDEs by super massive black holes. In this thesis I investigate lightcurves of both, TDEs by super massive and intermediate mass black holes. Finally, I will provide an outlook.

2 The *eROSITA* Mission

The extended ROentgen Survey with an Imaging Telescope Array (shortly *eROSITA*) is a German X-ray Telescope (Predehl et al., 2006, 2007, 2010, 2016) which was developed and built by the Max-Planck Institute for extraterrestrial Physics. It is planned to be the successor of the failed *ABRIXAS* (Predehl, 1999) and the canceled *ROSITA* mission (Predehl et al., 2003) and will be launched on board the Russian *Spektrum-Roentgen-Gamma* (*SRG*) satellite (Pavlinsky et al., 2008) in fall 2018. *eROSITA* will be orbiting the sun at the Lagrange point L_2 , where the gravitational forces and the orbital motion of a body are balanced. A schematic view of the location can be seen in Fig. 2.1. The first four years *eROSITA* will perform an all-sky survey. After that at least three years of pointed observations are intended (Merloni et al., 2012).

The main goal of the *eROSITA* mission is to study current cosmological models (Predehl et al., 2006). The dark energy model will be tested and the large scale structure of the universe as well as the evolution of black holes will be studied. Therefor the detection of 50–100 thousands of clusters of galaxies up to a redshift of $z > 1$ is aimed (Predehl et al., 2006). These clusters can be detected via the radiation of the hot intergalactic gas in their centers. To achieve the detection of such a large number of galaxy clusters a large effective area at low energies is needed. As *eROSITA* is sensitive in the energy range 0.2–10 keV (Predehl, 2012) it is designed for this task.

2.1 Technical details

A schematic diagram of the *eROSITA* telescope structure can be found in Fig. 2.2. The *eROSITA* instrument consists of seven detectors, more precisely Wolter-I mirror modules (Wolter, 1952a,b) which are arranged in a hexagonal manner. Each of them has 54 mirror shells made of gold-coated Nickel with an outer diameter of 358 mm (Merloni et al., 2012). The fact that there are seven detectors provides not only a seven-fold redundancy but also yields a lower background and pileup rate than a single, large telescope would have. For an on-axis detection the angular resolution, more precisely, the Half Energy Width (HEW) at 1.5 keV, is $\leq 15''$ (Merloni et al., 2012). The resolution characterizes how “pointlike” a point source is imaged on the focal plane. A non ideal optics allows the photons to scatter and thereby make the point source seem spread. The HEW is determined by a circle around the ideal image that contains half of the detected counts of the point source. In order to avoid single reflections from the rear end of the hyperboloid caused by a bright source just outside the field of view, a X-ray baffle is used. As the mirror system could get deformed with deviating temperature, during the operation the temperature has to be maintained at $20 \pm 2^\circ\text{C}$ to avoid image degradation (Merloni et al., 2012). In combination with the Wolter-I mirror modules CCD-cameras are used. The pixel size of these CCDs is $75 \mu\text{m}$ (Meidinger et al., 2011). 384×384 pixels build up one CCD. This size corresponds to an image area of $28.8 \text{ mm} \times 28.8 \text{ mm}$ (Merloni et al., 2012). The field of view is 1.03°

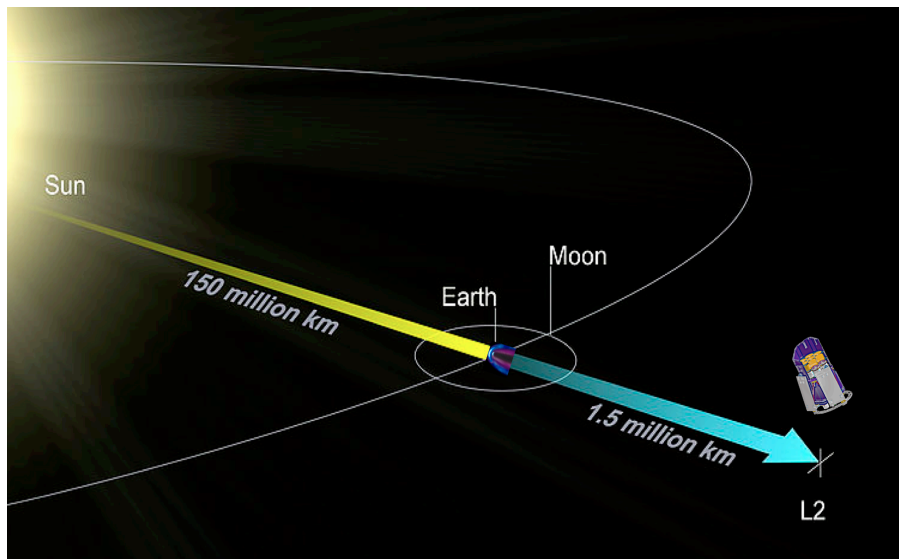


Figure 2.1: Schematic view of the location of the Lagrange point L_2 orbit of SRG (taken from Merloni et al., 2012).

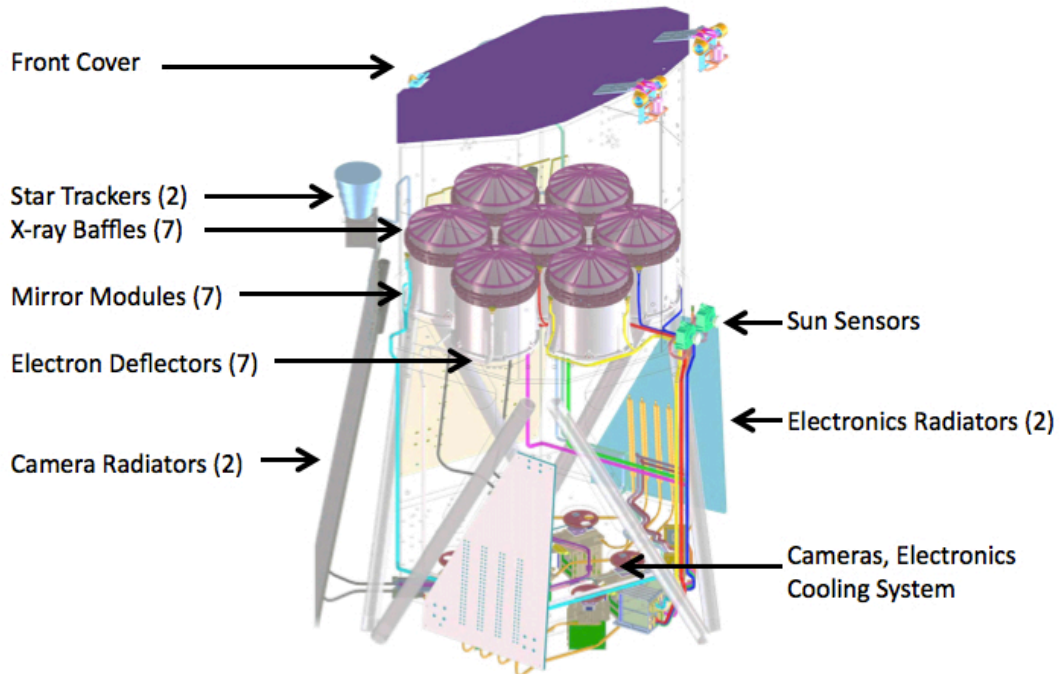


Figure 2.2: Schematic diagram of the *eROSITA* telescope structure (taken from Merloni et al., 2012).

Table 2.1: Summary of the technical details of *eROSITA* (Merloni et al., 2012)

mirror modules	7
mirror shells per module	54
energy range	0.2–10 keV
outer diameter	358 mm
angular resolution (at 1.5 keV)	$< 15''$ on axis
CCD size	384×384 pixels
CCD pixel size	$75 \mu\text{m}$
nominal integration time	50 ms
focal length	1.6 m

in diameter (Merloni et al., 2012). The nominal integration time was reduced to 50 ms (Merloni et al., 2012). This fact reduces the amount of out of time events during read out, when a photon hits the CCD-camera right during the read out phase. For shielding against particle radiation a massive copper housing surrounds the entire CCD-module. Furthermore, a graded shield consisting of aluminium and boron carbide or beryllium, respectively, is used to minimize fluorescence effects caused by cosmic rays (Merloni et al., 2012). *eROSITA*'s sensitivity in the soft X-ray band (0.5–2 keV) is 20–30 times higher than its precursor *ROSAT* (Merloni et al., 2012; Predehl et al., 2016). In the hard X-ray band (2–10 keV) it will even be the first survey of the entire sky at these energies.

2.2 X-ray telescopes and detectors

At this point it is useful to make a brief insertion of information on X-ray telescopes and detectors. Further information can be found in Krauss (2016, and references therein).

2.2.1 Wolter telescopes

Due to the small wavelength of X-ray radiation the critical reflection angle is small, too. Therefore, two mirrors are used to focus the incoming light to a focal point. As the photons are reflected at small angles, this type of mirror is called a “grazing incidence telescope”. Instead of two parabolic mirrors, as they are used in the optical, for X-ray wavelength paraboloids are combined with hyperboloids. The combination of both allows to shorten the focal length below ~ 10 m. This type of mirror is called a Wolter telescope (Wolter, 1952a,b). The shorter wavelength facilitates a launch on a rocket, which is necessary as the atmosphere is opaque for X-ray radiation. In addition, several mirror shells are nested to increase the effective area of the mirrors.

2.2.2 X-ray CCDs

As the photons are focused by the mirror module, something is needed to detect them. Therefore charge-coupled devices (CCDs) are used. In principle X-ray CCDs work the same as optical CCDs. However, because of the higher energy and the resulting larger penetration depths, a larger detector volume is needed. CCDs make use of the mechanism of a pn-junction. Incident X-ray photons excite electron-hole-pairs, which can be read out

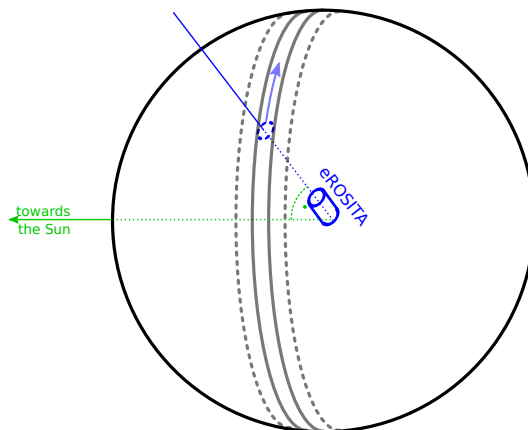


Figure 2.3: During the all-sky survey phase *eROSITA* scans the celestial sphere in approximate great circles. As the scan axis is facing the sun the great scanning circles are precessing. And due to the motion of the satellite around the sun the entire sky is covered once in a half year (taken from Schmid, 2012).

via transferring the electrons to the point where the read out happens. In this way it is possible to determine the individual location of an incoming photon and its energy.

2.3 All-sky survey and observing strategy

One all-sky survey by *eROSITA* takes half a year (Merloni et al., 2012). So in the four years of surveying the sky *eROSITA* will be doing eight surveys of the entire celestial sphere. A scheme of the survey strategy can be seen in Fig. 2.3. *eROSITA* will be scanning the sky in great circles which take 4 h (Merloni et al., 2012) and which all overlap at the ecliptic poles. This overlap is caused by the fact that the rotation axis is pointing towards the sun (Merloni et al., 2012). This means that the celestial sphere is relatively uniform covered with the exception of the ecliptic poles. But the rotation axis is only almost directly facing the sun. The small tilt of the rotation axis leads to a shift of the deepest exposures away from the ecliptic poles towards the galactic ones (Predehl et al., 2006). When the all-sky survey phase is completed, an average exposure of ~ 2.5 ksec will be reached if an observing efficiency of 100% is assumed. For more details on how that average exposure is calculated see Merloni et al. (2012). Fig. 2.4 shows the exposure map after the four years of surveys. The brightness of a pixel decodes its exposure time.

Since a source is scanned at least in six consecutive revolutions per 6-month all-sky survey and two of the six consecutive scans are separated by about 4 h, *eROSITA* is also capable to detect time variable phenomena on these timescales. Furthermore, as each point is scanned again half a year later, variability on timescales of months can be detected as well. In this way, for example, a tidal disruption event can be recognized latest after the second scan via the decrease in luminosity. In the next section the theory behind tidal disruption events is explained.

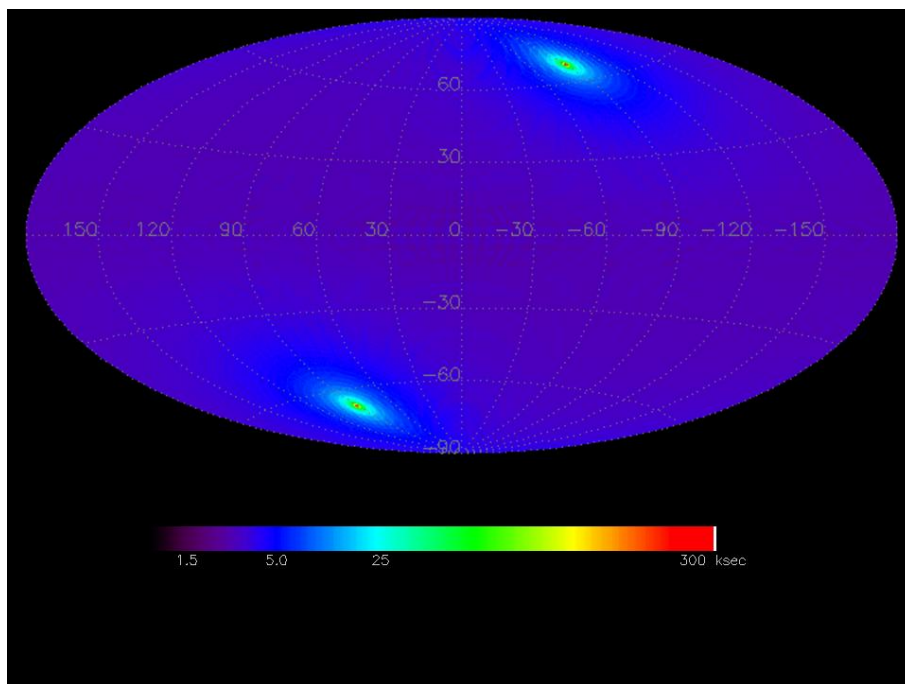


Figure 2.4: Exposure map after the four years of *eROSITA*'s all-sky survey (taken from <http://www.mpe.mpg.de/455799/instrument>). The brighter a pixel the higher is the exposure time.

3 Theoretical background - TDEs

Tidal disruption events have been first discovered in the 1990s by *ROSAT* (e.g. Bade et al., 1996). Since then, they were detected with *XMM-Newton*, *Chandra* and *Swift* as well as with, e.g., *GALEX* (e.g., Esquej et al., 2007; Maksym et al., 2010; Cenko et al., 2012; Gezari et al., 2006). Over 20 candidates for TDEs are known to date (see Komossa, 2015, for a rather complete list).

The interesting question is, how do these events arise and what does characterize them? If a star approaches the immediate vicinity of a super massive black hole (SMBH) it can be ripped apart by the tidal forces of the black hole. Due to the subsequent accretion of a significant fraction of the stellar material a luminous flare of electromagnetic radiation is produced (Komossa, 2015). This emission peaks in the UV or soft X-rays and declines on the timescale of months to years (e.g., Evans & Kochanek, 1989). The X-ray peak luminosity can go up to several 10^{44} erg s⁻¹ and the decline in lightcurves follows a $t^{-5/3}$ law (Komossa, 2015), as it is predicted by theory (Rees, 1988, 1989, for correction of the exponent). But not all debris of the star will be bound and eventually be accreted. A fraction of the stellar material can get on unbound orbits and escape (Komossa, 2015). Tidal disruption events can trace super massive black holes at the cores of galaxies which would be quiescent otherwise.

A scheme of a tidal disruption event can be seen in Fig. 3.1. The schematic drawing shows how the star gets distorted before it is disrupted. Additionally almost half of the debris would escape with high speeds. In Fig. 3.2 an artist's impression of the same is shown. The single steps of the TDE are labelled here.

First predictions of the occurrence of TDEs date back to the 1970s, based on theoretical considerations (e.g., Hills, 1975; Frank & Rees, 1976; Lacy et al., 1982; Evans & Kochanek, 1989). Detections started in the 1990s during the *ROSAT* all-sky survey and until now there have also been follow-up observations of some of the tidal disruption candidates (e.g., Komossa, 2015; Esquej et al., 2008; Saxton et al., 2012b; Lin et al., 2015).

There are a few properties that all TDEs show. During the high states the X-ray spectra are very soft, but a spectral hardening on the timescale of years follows (Komossa, 2015). Another property that all TDEs have in common is that the host galaxies show essentially no evidence for permanent activity. Years before and after the flare they are inactive, as well in the optical as in the radio and X-ray band. The masses of the SMBHs are mostly on the order of 10^6 – $10^8 M_\odot$ (Komossa, 2015).

A star is disrupted once the tidal forces of the SMBH exceed the self-gravity of the star (Hills, 1975). One can define a tidal radius, i.e., the distance at which the disruption happens,

$$R_t \approx 7 \times 10^{12} \left(\frac{M_{\text{BH}}}{10^6 M_\odot} \right)^{\frac{1}{3}} \left(\frac{M_*}{M_\odot} \right)^{-\frac{1}{3}} \frac{R_*}{R_\odot} \text{ cm} \quad (3.1)$$

(Komossa, 2015). Here M_{BH} denotes the mass of the black hole, M_* and R_* the mass and the radius of the disrupted star, respectively, and M_\odot and R_\odot the mass and the radius of

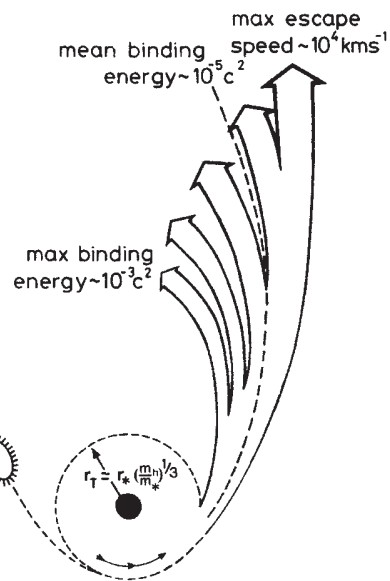


Figure 3.1: Schematic drawing of the tidal disruption of a solar-type star. Before disruption the star is distorted. Almost half of the debris would escape with speeds up to $\sim 10^4 \text{ km/s}$ (taken from Rees, 1988).

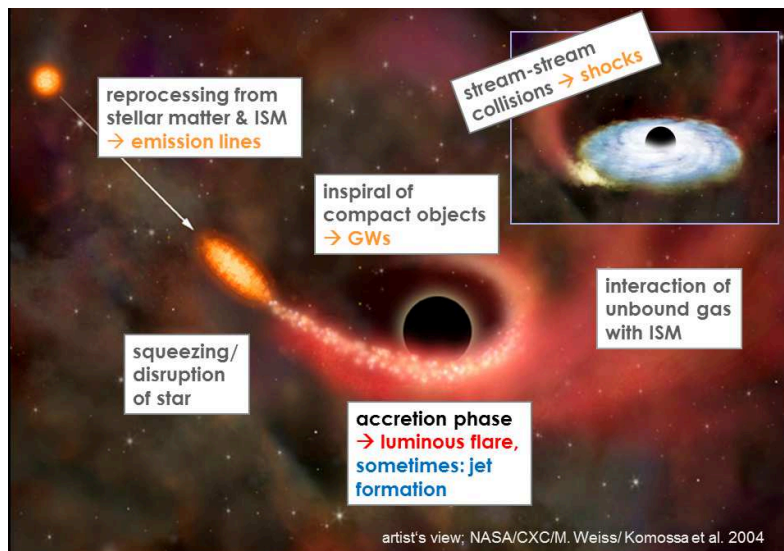


Figure 3.2: Artist's impression of the sites and sources of radiation during the evolution of a TDE. Note that only few TDEs launch radio jets (taken from Komossa, 2015).

the sun, respectively. By inserting the solar radius of about 7×10^8 m (Pehle & Waschi, 2011) one can find an even shorter description:

$$R_t = \left(\frac{M_{\text{BH}}}{M_*} \right)^{\frac{1}{3}} R_* \approx 23 R_S M_6^{-\frac{2}{3}} \quad (3.2)$$

(Lodato et al., 2015). For the last approximation a solar type star was assumed. R_S represents the Schwarzschild radius of the black hole, given by

$$R_S = \frac{2 G M_{\text{BH}}}{c^2} \quad (3.3)$$

with the gravitational constant $G \approx 6.7 \times 10^{-11} \text{ m}^3 \text{ kg}^{-1} \text{ s}^{-2}$ and the speed of light $c \approx 3 \times 10^8 \text{ m s}^{-1}$ (Pehle & Waschi, 2011). M_6 is an abbreviation for $M_{\text{BH}}/(10^6 M_\odot)$. To see that the last approximation is correct, one has to insert R_S and M_6 and then verify

$$23 \cdot \frac{2 G}{c^2} \cdot M_\odot \approx R_\odot \quad (3.4)$$

right by inserting the values. The last equation says that tidal disruption events occur close to the event horizon of the black hole. Due to this fact relativistic effects should be considered. One interesting point is that for SMBHs more massive than $10^8 M_\odot$ no TDE can occur as the tidal radius lies within the event horizon (Lodato et al., 2015). If relativistic effects are included, this limit can be raised to $10^9 M_\odot$ (Kesden, 2012).

Now it is possible to define another physical variable: the penetration factor. For R_p representing the pericenter of the orbit of the star, which is usually assumed to be parabolic, the penetration factor is defined by $\beta = R_t/R_p$ (Lodato et al., 2015). It characterizes how close a star gets to the black hole.

Furthermore, the strength η of the tidal encounter can be characterized as the square root of the ratio of the surface gravity of the star and its tidal acceleration at pericenter:

$$\eta = \left(\frac{R_p^3}{G M_{\text{BH}} R_*} \frac{G M_*}{R_*^2} \right)^{\frac{1}{2}} \quad (3.5)$$

(Evans & Kochanek, 1989). This is also the fraction of mass that the black hole retains from the disrupted star (Phinney, 1989).

To investigate tidal disruption events further and to finally get a mass fall back rate onto the black hole, one has to consider the energy of the star. At the disruption the orbital energy of the star is reduced by its binding energy, which is given by

$$E_b \approx \frac{G M_*}{R_*} \quad (3.6)$$

(Evans & Kochanek, 1989). The binding energy is much smaller than the specific kinetic energy at pericenter

$$E_0 = \frac{G M_{\text{BH}}}{R_p} = 10^4 E_b \quad (3.7)$$

(Evans & Kochanek, 1989). The spread in specific energy can be determined via the

change in the black hole's potential across a stellar radius:

$$\Delta E \approx \frac{G M_{\text{BH}}}{R_p} \frac{R_*}{R_p} = \frac{R_*}{R_p} \cdot E_0, \quad (3.8)$$

which is much larger than the binding energy (Evans & Kochanek, 1989). Therefore, nearly half of the mass of the disrupted star remains on bound orbits and half is ejected (Lacy et al., 1982). Evans & Kochanek (1989) estimated a mass distribution of the debris of

$$\frac{dM}{dE} \approx \frac{M_*}{2 \Delta E}, \quad (3.9)$$

but in simulations they observed a spread in energy of $1.8 \Delta E$ and a nearly constant mass distribution with

$$\frac{dM}{dE} \approx \frac{M_*}{1.8 \Delta E}. \quad (3.10)$$

One basic assumption of the theory of tidal disruption is that the bound debris of the disrupted star follows Keplerian orbits (Rees, 1988), i.e., only the point-like gravitational attraction of the black hole and the star are considered and every additional perturbation or interaction is neglected. These Keplerian orbits have different periods, which depend on their depth within the black hole's potential well. Using now the Keplerian relation

$$\frac{dE}{dt} = \frac{1}{3} (2\pi G M_{\text{BH}})^{\frac{2}{3}} t^{-\frac{5}{3}} \quad (3.11)$$

(Evans & Kochanek, 1989) one can determine the mass fall back rate

$$\dot{M} = \frac{dM}{dt} = \frac{dM}{dE} \frac{dE}{dt} = \frac{M_*}{3 t_{\text{min}}^{\frac{2}{3}}} \left(\frac{t}{t_{\text{min}}} \right)^{-\frac{5}{3}}, \quad (3.12)$$

where

$$t_{\text{min}} = \frac{\pi}{\sqrt{2}} \left(\frac{R_t}{R_*} \right)^{\frac{3}{2}} \sqrt{\frac{R_t^3}{G M_{\text{BH}}}} \approx 41 \sqrt{M_6} \text{ d} \quad (3.13)$$

(Lodato et al., 2015). In the formula for t_{min} the development in the theory of tidal disruption is already included. One could wonder why everywhere before the pericenter radius R_p is used whilst here the tidal radius R_t is used. This is because at the beginning of tidal disruption theory the disruption was thought to happen at R_p . As development went on, R_t was introduced as the point of disruption.

In equation 3.12 the assumption is that the relative width of the black hole's potential well at the tidal radius determines the spread of mechanical energies in debris (Sari et al., 2010; Guillochon & Ramirez-Ruiz, 2013; Stone et al., 2013). This assumption leads to the prediction that the peak accretion rate is significantly above the Eddington level for, e.g., a $10^6 M_{\odot}$ mass black hole. For a more massive black hole the peak rate is only moderately super-Eddington or can even become sub-Eddington to high enough masses (Lodato et al., 2015).

The Eddington limit is the theoretical maximal luminosity a radiating body can achieve. At the Eddington luminosity there is hydrostatic equilibrium, i.e., there is a balance between the radiation pressure, which is acting outward, and the gravitational force, which

is acting inward. The Eddington luminosity can be estimated via

$$L_{\text{Edd}} = 1.3 \times 10^4 M_6 \text{ erg s}^{-1} \quad (3.14)$$

(Evans & Kochanek, 1989).

Furthermore, the luminosity of a source is thought to be proportional to the mass fallback rate, more precisely,

$$L = \epsilon \dot{M} c^2 \quad (3.15)$$

(Khabibullin et al., 2014), where ϵ denotes a constant radiative efficiency. Therefore, the observed luminosity (and flux) scales as well as the mass fallback rate with $t^{-5/3}$.

But Lodato et al. (2009) realized that above fallback rate is only appropriate at late times. The early evolution of the system and the early rise of the lightcurve in contrast depend on the structure of the disrupted star. As Lodato et al. (2009) show, more incompressible stars have a sudden rise and more compressible ones a more gentle rise. This gentle or sudden rise is almost immediately followed by the canonical $t^{-5/3}$ decline.

On the other hand in case of a partial disruption the fallback rate at late times becomes much steeper as the mechanical energy is retained by the star (Guillochon & Ramirez-Ruiz, 2013) and thus there is a progressive lack of material with small mechanical energy.

But it is not only possible to state a simple proportionality for the luminosity but even kind of a real equation. To get to this description one has at first to think about some characteristic times. The first one is the time τ_i at which the peak mass rate occurs. For a solar-type star with a pericenter distance $R_p = 3R_S$ this is given by

$$\tau_i = 20 \left(\frac{M_{\text{BH}}}{10^6 M_\odot} \right)^{5/2} \text{ min} \quad (3.16)$$

after the instant of disruption t_0 (Khabibullin et al., 2014). In the early phase accretion takes place in an relatively inefficient regime and hence the luminosity is approximately constant $L = L_{\text{Edd}}$ and emitted by a thick accretion disc (Khabibullin et al., 2014; Strubbe & Quataert, 2009). The boundary between this early Eddington-phase and the late decay phase lies for $R_p = 3R_S$ at

$$\tau_{\text{Edd}} = 0.1 \left(\frac{M_{\text{BH}}}{10^6 M_\odot} \right)^{2/5} \text{ yr} \quad (3.17)$$

after disruption (Khabibullin et al., 2014). A simplified relation for the time dependency of the luminosity is given by

$$L(t) = \begin{cases} L_{\text{quies}} & \text{for } t < t_0 \\ L_0 & \text{for } t_0 < t < t_1 \\ L_0 \left(\frac{t-t_0}{\tau_{\text{Edd}}} \right)^{-5/3} & \text{for } t > t_1 \end{cases} \quad (3.18)$$

(Khabibullin et al., 2014), where L_{quies} is the source luminosity in a quiescent state, $L_0 = \zeta L_{\text{Edd}} \gg L_{\text{quies}}$ is the observed peak luminosity, and $t_1 = t_0 + \tau_{\text{Edd}}$. ζ denotes a geometrical dilution factor. In this formula for simplification the short period of time when $\tau_i \ll \tau_{\text{Edd}}$ is ignored although it could be possible to detect a TDE right in its rising phase.

It should be mentioned that only the lightcurve in soft X-rays is expected to follow the canonical $t^{-5/3}$ decline in flux. At optical/UV wavelength the emission of the accretion disc sits in the Rayleigh-Jeans part of the spectrum and should therefore evolve as the temperature that scales with

$$\dot{M}_{\text{fb}}^{1/4} \propto t^{-5/12} \quad (3.19)$$

(Lodato et al., 2015). Although it is not expected, the optical lightcurve in many cases does show a canonical $t^{-5/3}$ decline (Gezari et al., 2009, 2012). For this reason there is ongoing development in modelling the emission (Guillochon et al., 2014).

The rate of tidal disruptions depends on several factors, e.g., it is enhanced in some phases of binary SMBH evolution (e.g., Chen et al., 2009) or it depends on BH spin for the most massive BHs ($M > 10^8 M_{\odot}$) (Kesden, 2012). The suggestions for the tidal disruption rate range between 10^{-4} and 10^{-5} per galaxy and year, in agreement with theoretical order-of-magnitude predictions (Komossa, 2015, and references therein). Further, TDEs probably contributed to SMBH growth (Freitag & Benz, 2002).

There are various applications making use of the characteristic properties and rates of TDEs. For example, in X-rays they can probe relativistic effects or provide a new means to measure BH spin. Furthermore, jetted TDEs can give new insight into the formation and early evolution of radio jets, although most TDEs do not launch powerful radio jets. Additionally TDEs in gas-rich environment will illuminate the circumnuclear material and therefore provide us an opportunity of reverberation mapping the cores of quiescent galaxies (Komossa, 2015).

4 Data analysis

To improve my knowledge about TDEs I analyzed the spectra of two known sources. I chose NGC 3599 and Swift J2058.4+0516. Both are among the brightest of the known tidal disruption candidates.

4.1 NGC 3599

4.1.1 Source description

NGC 3599 can be classified as an early-type galaxy in the local Universe with a redshift of $z = 0.0028$ (Esquej et al., 2012). Its position is ($\alpha_{2000} = 11^{\text{h}}15^{\text{m}}26.^{\text{s}}9$, $\delta_{2000} = +18^{\circ}06'37''$) (Saxton et al., 2015). It was discovered in a *XMM-Newton* slew from 2003 with a soft X-ray flux, which was a factor >100 higher than an upper limit from *ROSAT* (Esquej et al., 2007). Further observations of this galaxy by *XMM-Newton*, *Chandra*, and *Swift* revealed a strong decay in flux by a factor ~ 100 over the following years (Esquej et al., 2008, 2012). A possible explanation for this behavior is a tidal disruption event. Additionally NGC 3599 shows weak narrow, optical lines, which led to a classification as a low-ionization nuclear emission-line region (LINER) or Seyfert 2 galaxy (Esquej et al., 2008).

4.1.2 Observational details

Here a *XMM-Newton*/EPIC pointed observation (ObsID 0556090101) of NGC 3599 was used. It was taken on 2008 December 2 with an exposure of about 40 ks. All EPIC-pn and MOS exposures were taken in Full Frame mode with the medium filter (Esquej et al., 2012).

4.1.3 Data reduction

A standard source detection analysis was performed with the help of the command `xmextract`. In principle at first calibrated photon event files for the MOS cameras as well as for the PN camera are produced. After that an image is created. Such an image for the PN detector can be seen in Fig. 4.1. This image provides an overview of what was detected and how the source one is interested in looks like. After that filters can be applied, for example to exclude pattern pileup. Additionally it is possible to filter on time using Good Time Intervals (GTIs). Now source and background spectra can be extracted. For PN and MOS2 source photons were extracted from a circular region of $15''$ radius centered on the object position. For MOS1 a radius of $13''$ was used. For each detector a circular source-free region on the same chip and radius of $60''$ was used to determine the background. Finally the Photon Redistribution Matrix (RMF) and the Ancillary File (ARF)

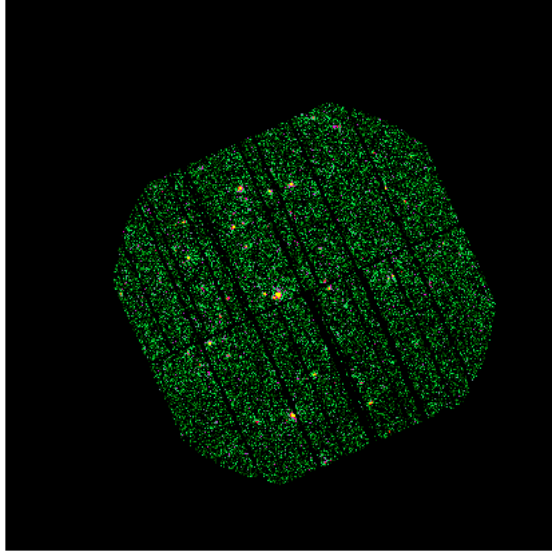


Figure 4.1: Image of the PN detector.

are produced which describe the detector response.¹

To decide whether pileup has to be taken into account, the observed count rate for each detector was calculated by dividing the number of total counts by the exposure time. The resulting values for the count rate are 0.028 counts s⁻¹ (PN), 0.005 counts s⁻¹ (MOS1), and 0.006 counts s⁻¹ (MOS2), respectively. According to the *XMM-Newton* Users Handbook² the maximal count rate in full frame mode for PN is 2 counts s⁻¹ and for both MOS-detectors 0.5 counts s⁻¹. Above these values pileup has to be taken into account. This means for my data analysis pileup is not important and no pileup correction has to be performed.

4.1.4 Data analysis

For all data analyses done here the ISIS-version 1.6.2-37 was used.

The background subtracted spectra were at first binned to a minimum signal to noise ratio of 4. Furthermore, only counts between 0.1 and 10 keV are used for the analysis.

At first I wanted to test the best fit model of Esquej et al. (2012). They used the same *XMM-Newton* observation of NGC 3599 as is used here and additionally a *XMM-Newton* Target of Opportunity observation as well as a *Chandra* pointed observation. Their best fit was obtained with a power law plus a black body with photon index $\Gamma_X = 2.70^{+0.33}_{-0.30}$ and $kT = 44^{+19}_{-17}$ eV. The formula for this fit function is given by

$$A(E) = K_1 \left(\frac{E}{1 \text{ keV}} \right)^{-\Gamma_X} + K_2 \cdot \frac{8.0525 E^2 dE}{kT^4 \left(\exp \left(\frac{E}{kT} \right) - 1 \right)}, \quad (4.1)$$

¹for more information on the reduction process and the single steps see <https://heasarc.gsfc.nasa.gov/docs/xmm/abc/node8.html>.

²https://xmm-tools.cosmos.esa.int/external/xmm_user_support/documentation/uhb/epicmode.html.

where K_1 and $K_2 = L_{39}/D_{10}^2$ represent the normalization of the power law in photons $\text{keV}^{-1} \text{cm}^{-2} \text{s}^{-1}$ at 1 keV and black body respectively. L_{39} is the source luminosity in units of $10^{39} \text{erg s}^{-1}$ and D_{10} the distance of the source in units of 10 kpc. For details to the fit functions see the Heasarc XSPEC Manual³.

For my first fit I froze the parameters to the values of Esquej et al. (2012). The resulting reduced χ^2 for the simultaneous fit of the PN and both MOS data is 1.21/62. The latter number represents the degrees of freedom. The normalization of the power law and the black body is $(9.3 \pm 0.5) \times 10^{-6} \text{photons keV}^{-1} \text{cm}^{-2} \text{s}^{-1}$ at 1 keV and 0 (at least $\leq 1.2 \times 10^{-7}$) $10^{39} \text{erg s}^{-1} (10 \text{kpc})^{-1}$ respectively. The flux was calculated with the ISIS-function `model_flux` in the energy range 0.1 to 10 keV and then averaged over the thus determined fluxes for pn and both mos. The resulting averaged flux for the 0.1–10 keV band is $1.02 \times 10^{-13} \text{erg cm}^{-2} \text{s}^{-1}$. Additionally the significance of the black body component was calculated via an ISIS-function called `mc_sig` and determined to be 0.25. In principle this ISIS-function is doing Monte Carlo simulations of spectra data without the component that should be tested for (in this case the black body). This is done for each detector. Here I did 1 Million Monte Carlo loops. Then the simulated spectra are fitted with and without that component and the difference of the resulting χ^2 is calculated. In the next step this difference can be compared to the measured difference in χ^2 . If the simulated $\Delta\chi^2$ is greater than or equal to the measured one, this is called a “false positive” because here the value is greater just by accident as the spectra were simulated without that component tested for. If one counts these false positives for all simulations, one can determine the significance of that specific component of the model. As in my case the significance of the black body component is 0.25 there must be a big amount of fits to the simulated data, where the improvement of χ^2 is higher than the real one. This means therefore that the black body component does not significantly improve the fit.

As the normalization of the black body is 0 I tried a pure power law as fit function. All parameters were allowed to vary. The best fit with a reduced $\chi^2 = 1.16/62$ has a photon index $\Gamma_X = 2.59_{-0.10}^{+0.11}$ and a normalization of $(9.8 \pm 0.7) \times 10^{-6} \text{photons keV}^{-1} \text{cm}^{-2} \text{s}^{-1}$ at 1 keV. This photon index is close to that of Esquej et al. (2012) but produces a slightly better reduced χ^2 . The 0.1–10 keV flux of $9.62 \times 10^{-14} \text{erg cm}^{-2} \text{s}^{-1}$ is determined in the same manner as above.

The plots of both fits, the power law plus black body as well as the pure power law, are shown in Fig. 4.3. Panel a) shows the power law plus black body fit with frozen parameters to the values of Esquej et al. (2012). The residuals can be found in panel b). In addition the contributions of the single components to the model are plotted as well. As one can see only the power law component has a major contribute to the fit and not the black body. My attempt at a pure power law fit is plotted in panel c) and the related residuals in panel d). Note the slightly smaller reduced χ^2 .

For comparison reasons I took the figure of the best fit of Esquej et al. (2012) out of their paper and show it right next to my results in Fig. 4.2. In the end, I was not able to confirm their resulting model. One possible explanation for this could be that I have more degrees of freedom. They do not state the number of degrees of freedom in their paper, so I can not compare them. Another and in my opinion more important explanation could be that Esquej et al. (2012) used more observations and fitted them simultaneously. As the observations were taken at different times – the XMM ToO-observation about two and a

³<https://heasarc.gsfc.nasa.gov/xanadu/xspec/xspec11/manual/node38.html>.

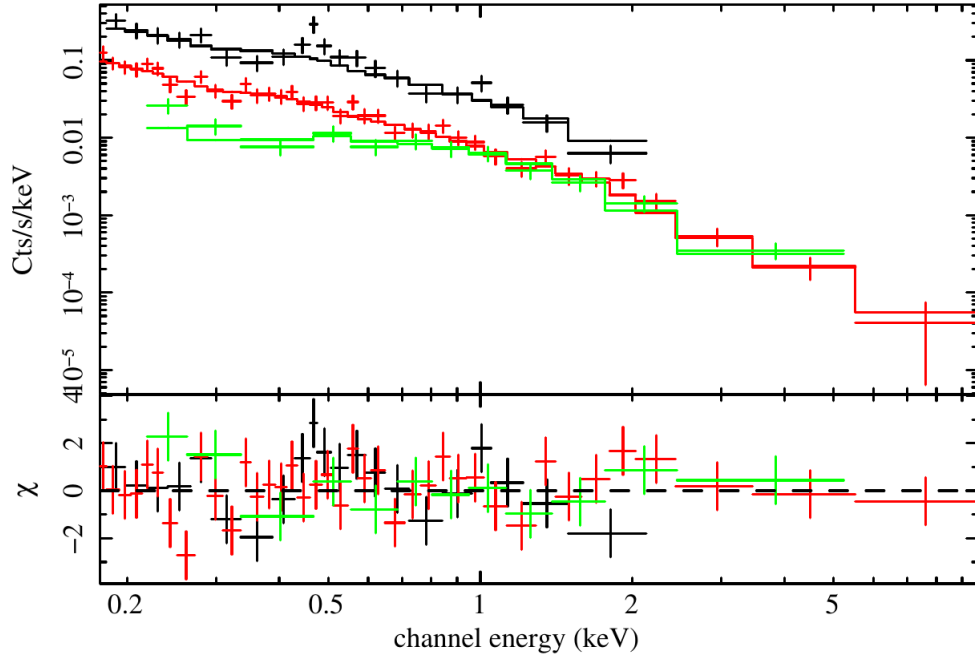


Figure 4.2: Best fit of Esquej et al. (2012). Black denotes a *XMM-Newton* EPIC-pn ToO, green a *Chandra* ACIS-S spectrum, and red a *XMM-Newton* X-ray spectrum of NGC 3599. The latter is the observation I analyzed.

half year and the *Chandra*-observation almost one year before the observation I analyzed here (see Esquej et al., 2012, for the exact dates) – a change in spectral shape can at least not be excluded.

4.2 *Swift* J2058.4+0516

4.2.1 Source description

The coordinates of this object are ($\alpha_{2000} = 20^{\text{h}}58^{\text{m}}19.^{\text{s}}898$, $\delta_{2000} = +05^{\circ}13'32''.25$)⁴ and the redshift of its host galaxy is $z = 1.1853$ (Cenko et al., 2012). It was discovered by the *Swift* Burst Alert Telescope (BAT, see Barthelmy et al., 2005, for details) in 2011 (Krimm et al., 2011). It is a long-lived, super-Eddington X-ray outburst with a luminous radio counterpart, which indicates presence of relativistic ejecta, and relatively faint optical emission (Cenko et al., 2012).

4.2.2 Observational details

Here a *Swift* target-of-opportunity (ToO) observation of Sw J2058+05 was analyzed. This observation (ObsID 00032004001) began on 2011 May 27⁵ and had an exposure time of about 3 ksec.

⁴<http://simbad.u-strasbg.fr/simbad>.

⁵<https://heasarc.gsfc.nasa.gov/cgi-bin/W3Browse/w3browse.pl>.

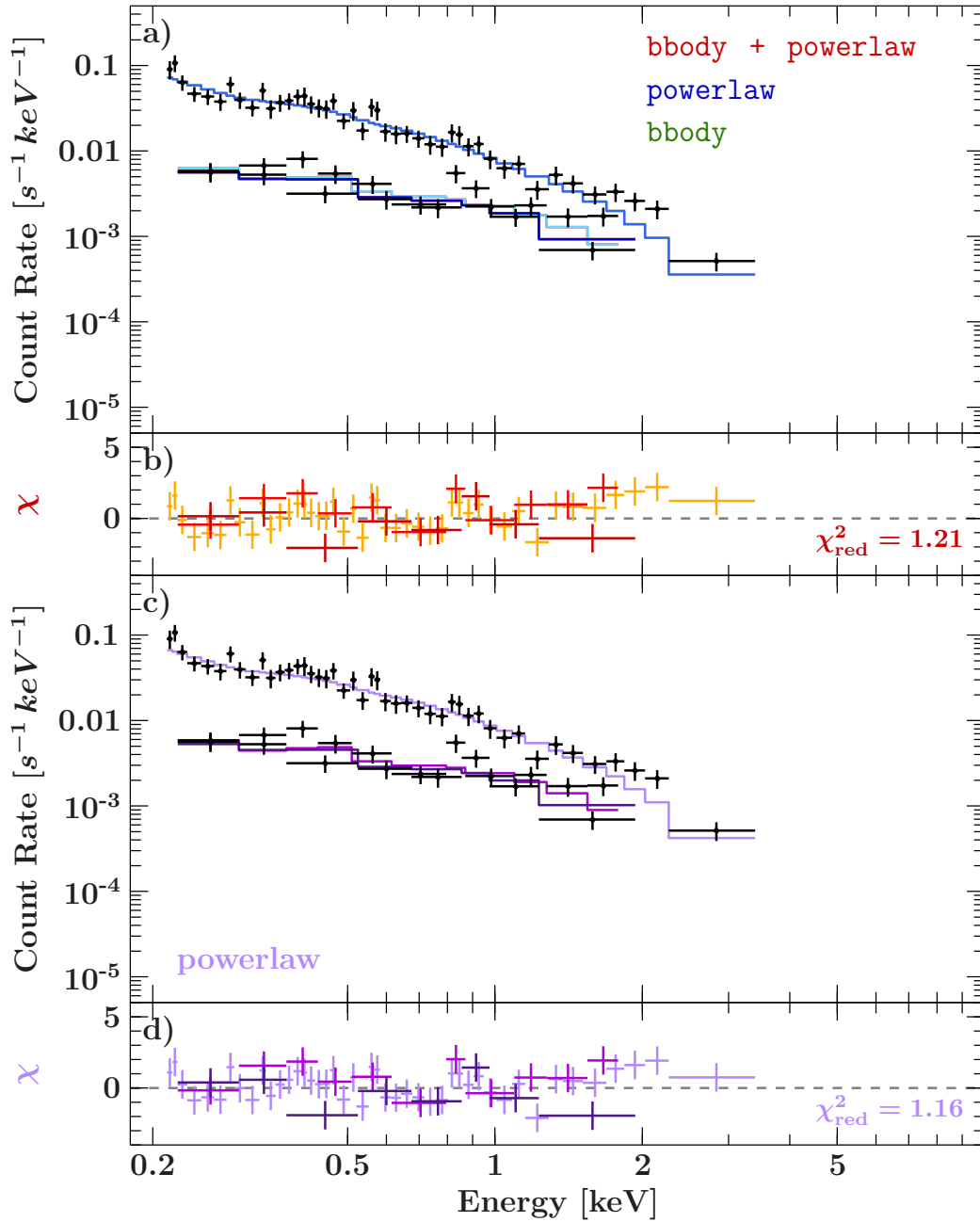


Figure 4.3: Panel a) shows the reproduced best fit of Esquej et al. (2012) with the contributions of the different components of the model; note that the black body component can not be seen here. Panel c) illustrates a pure power law fit with free parameters. Panels b) and d) show the residuals. Note the smaller reduced χ^2 of the pure power law fit.

4.2.3 Data reduction

For the source extraction a script written by Felicia Krauss was used. This script uses the `xrtextextract`-command. The single steps are similar to those described above. Source photons were extracted from a circular region with $35''$ radius centered on the object position. To determine the background an annulus with an inner radius of $35''$ and an outer radius of $50''$, centered on the object position as well, was applied.

4.2.4 Data analysis

The reduced spectrum was binned to a minimum signal to noise ratio of 5 and the energy range used for analysis was restricted to 0.2 up to 10 keV. For *Swift* data it is necessary to set the RMF OGIP compliance to 0 as the PHA-files coming out of the data reduction process deviate slightly from the OGIP standard.

As I did it for NGC 3599, I first attempted to reproduce the best fit of Cenko et al. (2012). For this reason I used an absorbed power law as fit function. As an absorption model I used the Tuebingen-Boulder Interstellar Medium (ISM) absorption model `tbabs`, which includes absorption due to the gas-phase ISM as well as the grain-phase ISM as well as the molecules in the ISM⁶. Therefore the fit formula is given by

$$A(E) = N_{\text{H}} \cdot K \left(\frac{E}{1 \text{ keV}} \right)^{-\Gamma_{\text{X}}}, \quad (4.2)$$

where N_{H} represents the equivalent hydrogen column, K the normalization of the power law and Γ_{X} the photon index. It is also important to set the abundance to the values of Wilms et al. (2000). To reproduce the fit of Cenko et al. (2012) I froze the equivalent hydrogen column N_{H} to $0.26 \times 10^{22} \text{ cm}^{-2}$ and the photon index Γ_{X} to 1.61. The resulting reduced χ^2 is 1.07/93. The latter number represents the degrees of freedom again. Cenko et al. (2012) had less degrees of freedom, more precisely, they state 54 degrees of freedom in their paper. The plot and residuals of my reproduced fit can be seen in the upper panels a) and b) of Fig. 4.4. As one can see it fits quite well. For the normalization of the power law I get $(7.47 \pm 0.25) \times 10^{-3} \text{ photons keV}^{-1} \text{ cm}^{-2} \text{ s}^{-1}$ at 1 keV. The measured flux in the 0.3–10 keV band is $4.56 \times 10^{-11} \text{ erg cm}^{-2} \text{ s}^{-1}$.

As there are some deviations around 0.5 keV I checked whether it improves the fit when N_{H} is not frozen to a certain value but left free. The result is only a slightly improved fit and can be seen as the blue line in panel c) of Fig. 4.4. The resulting reduced χ^2 is 1.06/92 and $N_{\text{H}} = 0.235_{-0.026}^{+0.030} \times 10^{22} \text{ cm}^{-2}$. This means it is a bit smaller than the value of Cenko et al. (2012). The flux in the 0.3–10 keV band can be determined to $4.50 \times 10^{-11} \text{ erg cm}^{-2} \text{ s}^{-1}$. Here the normalization of the power law is $(7.3 \pm 0.4) \times 10^{-3} \text{ photons keV}^{-1} \text{ cm}^{-2} \text{ s}^{-1}$ at 1 keV.

Because I did not find a black body component in the spectra of NGC 3599 I tried to model one here. Therefore I fitted an absorbed power law plus black body to the spectrum of *Swift* J2058.4+0516 and left all parameters free. The result can be seen as the green line in panel c) of Fig. 4.4. The value of the reduced χ^2 here is 0.79/89, i.e., it is under determined. For this fit the resulting 0.3–10 keV flux is $4.95 \times 10^{-11} \text{ erg cm}^{-2} \text{ s}^{-1}$ and the parameters are $N_{\text{H}} = 0.41_{-0.18}^{+0.19} \text{ cm}^{-2}$, $\Gamma_{\text{X}} = 1.518_{-0.023}^{+0.133}$, the normalization of the

⁶<https://heasarc.gsfc.nasa.gov/xanadu/xspec/xspec11/manual/node42.html#tbabs>.

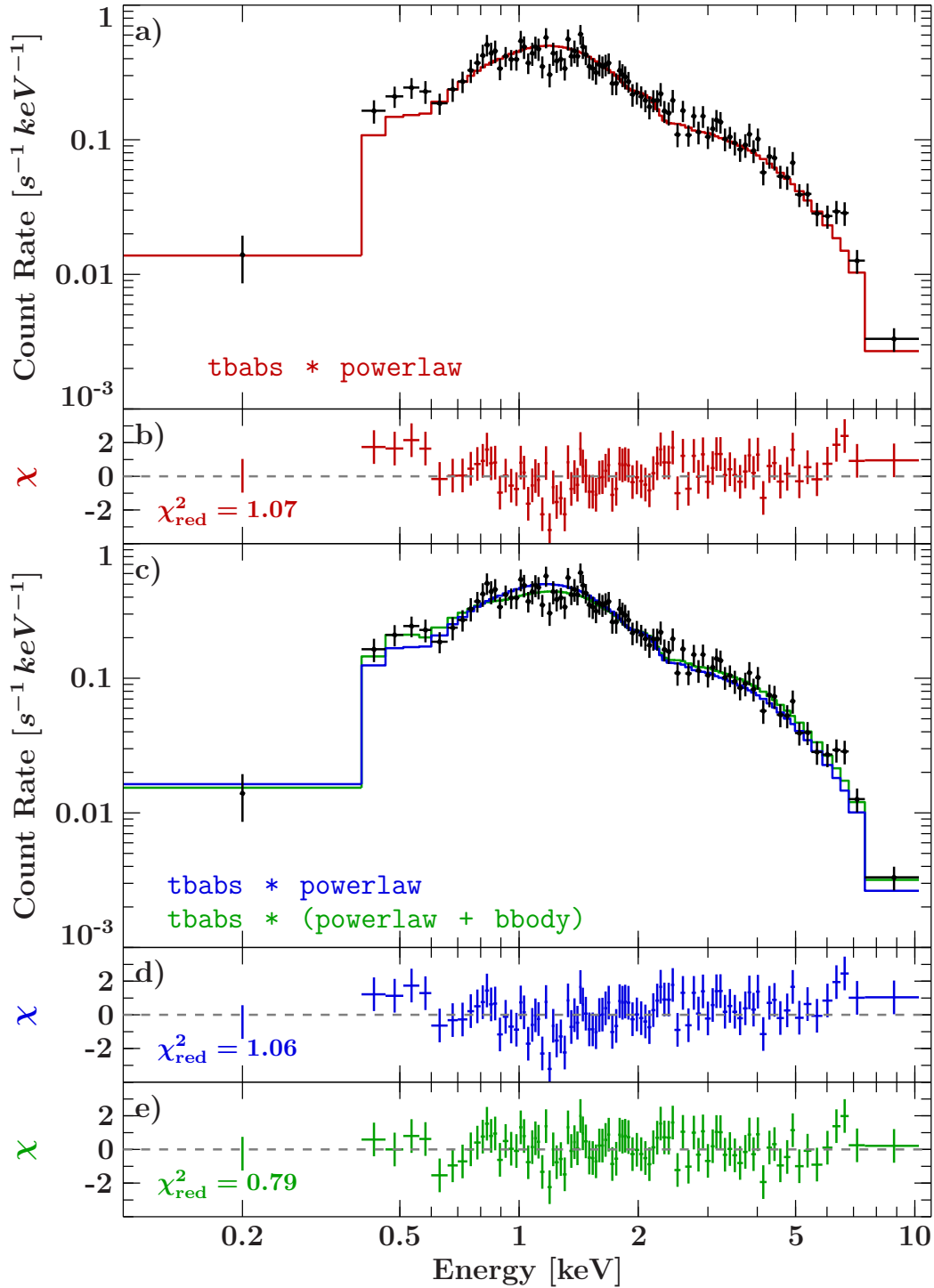


Figure 4.4: Panel a) shows the reproduced best fit of Cenko et al. (2012). In panel b) the residuals associated with this fit can be seen. Panel c) illustrates an absorbed power law fit with free parameter Γ_X as well as an absorbed power law plus blackbody. Panels d) and e) show the residuals.

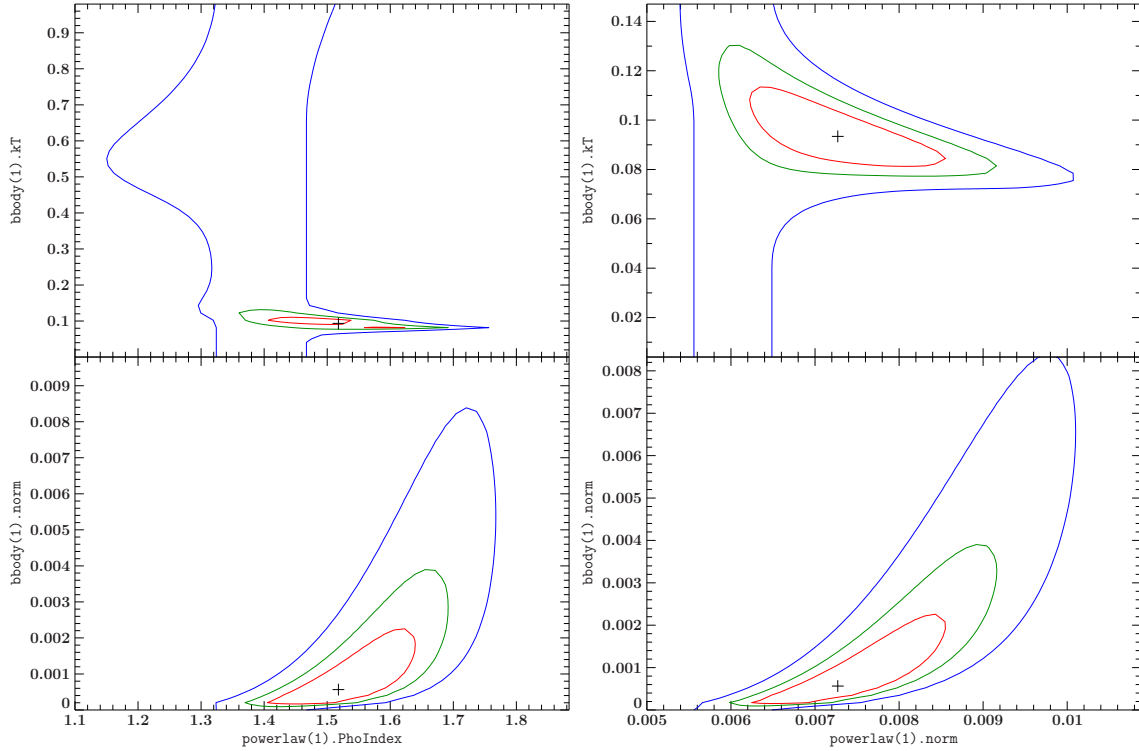


Figure 4.5: Contour plots for the black body plus power law fit. It is obvious that the parameters are correlated. The red line denotes 3σ , the green line 90% confidence, and the blue line 1σ . The x-axis of the left panel is the photon index of the power law and the one of the right panel the normalization of the power law. The y-axis of the upper panels is kT of the black body component and the one of the lower panel is the normalization of the black body.

power law is $(7.27^{+308.66}_{-0.25}) \times 10^{-3}$ photons $\text{keV}^{-1} \text{cm}^{-2} \text{s}^{-1}$ at 1 keV, $kT = 0.093^{+0.023}_{-0.014}$ keV, and the normalization of the blackbody is $(6^{+372532}_{-5}) \times 10^{-4} 10^{39} \text{ergs}^{-1} (10 \text{kpc})^{-1}$. The equivalent hydrogen column changes its value and there is a small change in the photon index. As the confidence intervals for the normalizations are large, I plotted contours of the errors. The results can be found in Fig. 4.5. The x-axis of the left panel is the photon index of the power law and the one of the right panel the normalization of the power law. The red line denotes 3σ , the green line 90% confidence, and the blue line 1σ . The y-axis of the upper panels is kT of the black body component and the one of the lower panel is the normalization of the black body. A correlation between the parameters is obvious. For example, the higher the power law photon index is, the higher is the normalization of the black body. Furthermore, a high photon index correlates with a low black body kT . But at least for 1σ confidence, for a photon index between 1.3 and 1.5 almost every black body kT seems to be possible.

To conclude, the data can be well described by an absorbed power law with the values found in Cenko et al. (2012). An absorbed power law plus black body describes the data also quite well but does not improve the fit, so it is not necessary to make the fit function more complicated.

5 The SIXTE-Software

After having analyzed two observed spectra of known TDEs, I can start the simulation part. But before doing so, I want to explain some basics of the simulation software.

5.1 SIXTE

The software package is called “SIMulation of X-ray TElescopes” (SIXTE). Among others, it can be used to simulate *eROSITA*’s all-sky survey. It was developed to perform mission-independent Monte Carlo simulations for astronomical X-ray instrumentations (Schmid, 2012). In the following I just want to give a brief overview of the basic elements of the software. Further information can be found in the SIXTE manual¹.

One effort of the software is that it provides realistic and accurate data within a reasonable amount of time. The main elements are the imaging and the detector module. The imaging module is responsible for modelling the X-ray optics, while the detector module can be adjusted for different instruments. But there are also auxiliary tools. A schematic layout of the simulation pipeline can be found in Fig. 5.1. In simple words one provides the software a source catalogue. Then SIXTE generates photons from the source by taking the effective area of the instrument and the attitude into account. In Sec. 5.2 I will explain what an attitude is. After that a photon list is created. This list contains the arrival time, the energy, and the position of the incoming photons in right ascension and declination. For the imaging process, the point-spread function (PSF), vignetting, and again the attitude are taken into account. The imaging process results in an impact list, which contains again the arrival time, the energy, and the position of the photons, but this time in detector coordinates. The next step is the photon detection. Therefore, the Redistribution Matrix File (RMF), charge cloud splitting, pileup, background, bad pixels, and the read-out mode are taken into account. Finally, one gets an event list with the read-out time, the measured energy and the pixel, which the photon hit. This event list can then be used to create an image, a spectrum, or a lightcurve. Or in general, this event

¹http://www.sternwarte.uni-erlangen.de/research/sixte/data/simulator_manual.pdf

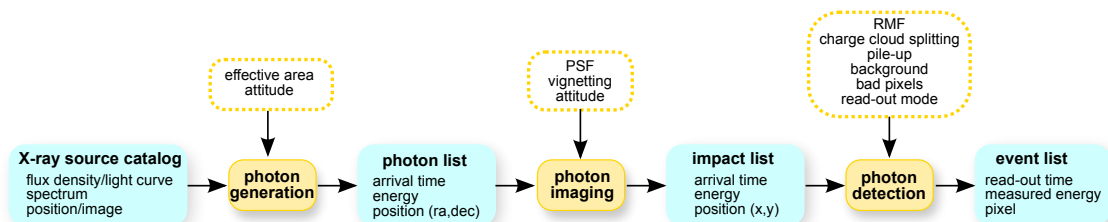


Figure 5.1: Schematic layout of the simulation pipeline (taken from Schmid, 2012).

list can then be analyzed. As *eROSITA* has seven telescopes, seven event lists are created. These seven event files can be merged together with the help of the FTOOL command `ftmerge`. The input for the simulation software is provided by a SIMPUT file, which is a standardized format for source descriptions as simulation input. In Sec. 5.3 I will give some more information about this special format.

5.2 erosim

For my simulations I used the software tool “erosim”. This tool needs some more parameters. In the following I describe a selection of them only briefly.

XMLFile: The XML file describes the behavior of the telescopes. For this reason, it contains many essential parameters of the detectors, e.g., the FOV diameter, the focal length, the ARF and RMF, the PSF, and the pixel size. Because there are seven detectors, there are seven XML files as well.

Attitude: *eROSITA* will be doing all-sky surveys. Therefore, a file is needed that describes at which point on the sky *eROSITA* is looking at a certain time. This is specified by the attitude file. If this file is not given, SIXTE will perform a pointed observation for the given exposure time. If it is given, the given coordinates (i.e., RA, DEC) are overwritten as they are useless in this case.

RA, DEC: These are the coordinates in the equatorial coordinate system. They are always required, but are ignored if an attitude file is provided.

SIMPUT: This file contains the required information on the sources.

MJDREF: The reference Modified Julian Date. Time will be given in the event files with respect to this date.

Exposure: This parameter denotes the time, which is simulated. It can be combined with a starting time given by TSTART. If a GTI file is given the exposure is overwritten.

GTIFile: GTI is the abbreviation for “Good Time Interval”. It contains starting and end times. With the help of this file one can define a time span when the source is in *eROSITA*’s field of view.

5.3 SIMPUT

The SIMulation inPUT (SIMPUT) file format specification is based on the FITS standard (Hanisch et al., 2001; Pence et al., 2010). A SIMPUT file is designed to describe one or more sources by giving information on the position, flux, and energy spectrum as well as optional spatial flux distribution and timing information (“lightcurves”). Furthermore, the main extension of a SIMPUT file is the source catalogue, called SRC_CAT. This extension is a table and contains the parameters that describe the sources. These parameters are:

SRC_ID	the ID of each source
SRC_NAME	the name of each source

RA, DEC	the coordinates of the source in the equatorial coordinate system
E_MIN, E_MAX	boundaries of the energy band in which the flux is given
FLUX	the flux emitted by the source in the specified energy band
SPECTRUM	a link to the spectrum extension
TIMING	a link to the timing extension (lightcurve)

A spectrum is required for each source. Contrary, a lightcurve is optional, but as TDEs are time dependent, it is given for all of my sources. Further information on SIMPUTs can be found in the definition document².

²<http://hea-www.harvard.edu/heasarc/formats/simput-1.1.0.pdf>.

6 Simulations for *eROSITA*

This section tries to use the above explained simulation software to answer some exciting questions concerning TDEs and the *eROSITA* mission. For example these exciting questions include, how a TDE observed by *eROSITA* would look like. Furthermore, I attempt to predict if it is possible to recognize a tidal disruption event within one day or if really a time span of half a year or longer is necessary to identify it. Another very interesting question is, whether the mass of the black hole plays a role in the detectability of these events.

6.1 Source catalogue

In order to answer these questions I first created a source catalogue. The sources I used can be found in Tab. 6.1. There I list the source name, its redshift, its flux in the 0.1–10 keV energy band, the ISIS fit function I used to describe the spectrum, and references, where one can find more information on these sources. Although it was not stated in every paper I used an absorbed spectral model for all sources. The absorption model I used is the same as in Sect. 4.2.4, the Tuebingen-Boulder Interstellar Medium (ISM) absorption model `tbabs` (Wilms et al., 2000). Note that the listed flux was determined by evaluating the fit function on a fine grid after all model parameters are set to the values which can be found in the reference papers and after the flux given in these papers was taken into account. The flux was often given in other energy bands than 0.1–10 keV. Therefore, I used the ISIS convolution model `enflux` to adjust the flux to the right value in the energy band given in the reference. After that I could determine the flux in the right energy range by evaluating the spectral model on a fine grid with the chosen energy limits.

The coordinates for each source are chosen randomly, uniformly over the entire sky. For the right ascension (RA) I used values between 0 and 360°, and for the declination (DEC) between 0 and 90°. Furthermore, I used random start times t_{start} at which the decay in flux begins. These times were chosen in a time range of half a year. In this way the lightcurves of the single sources began its decaying phase randomly one after each other. As F_0 I used the flux listed in table 6.1 although this is not always the peak flux.

For the first investigation of tidal disruption events I set the lightcurve as constant 0 for the case $t < t_{\text{start}}$. And for the case $t \geq t_{\text{start}}$ I chose a simple power law. Since the luminosity and the flux of a source are associated via

$$F = \frac{L}{4\pi d^2}, \quad (6.1)$$

where d is the distance from the observer to the source, describing the lightcurve by using

Table 6.1: Properties of the sources used for the simulations. Note that the flux was determined in the 0.1–10 keV band. For a detailed description of the fit models see <https://heasarc.gsfc.nasa.gov/xanadu/xspec/xspec11/manual/node38.html>.

source name	redshift	flux [erg s ⁻¹ cm ⁻²]	fit model	reference
NGC 3599	0.0028	3.19×10^{-11}	bbody	Esquej et al. (2008)
SwiftJ2058+0516	1.1853	7.90×10^{-11}	powerlaw	Cenko et al. (2012)
NGC 5905	0.011	2.61×10^{-11}	powerlaw	Bade et al. (1996)
RXJ1242.6-1119	0.05	1.52×10^{-11}	bbody	Komossa & Greiner (1999)
RXJ1624+7554	0.064	1.22×10^{-11}	powerlaw	Grupe et al. (1999)
RXJ1420+5334	0.147	7.90×10^{-12}	bbody	Greiner et al. (2000)
TDXF1347-3254	0.0366	8.10×10^{-13}	bbody	Cappelluti et al. (2009)
SDSSJ1311-0123	0.195	5.30×10^{-14}	bbody	Maksym et al. (2010)
2XMMi1847-6317	0.0353	1.76×10^{-12}	diskbb + powerlaw	Lin et al. (2011)
SDSSJ1201+3003	0.146	8.54×10^{-14}	zbremss	Saxton et al. (2012a)
WINGSJ1348	0.062	2.84×10^{-13}	powerlaw	Maksym et al. (2013)
RBS1032	0.026	7.70×10^{-14}	zpowerlw	Maksym et al. (2014)
3XMMJ1521+0749	0.17901	3.90×10^{-13}	edge · diskbb	Lin et al. (2015)

the flux is equivalent to using the luminosity. The formula of the lightcurve was

$$F(t) = \begin{cases} 0 & \text{for } t < t_{\text{start}} \\ \left(\frac{t-t_{\text{start}}+1}{1 \text{ yr}}\right)^{-5/3} F_0 & \text{for } t \geq t_{\text{start}} \end{cases} \quad (6.2)$$

By solving $\tau_{\text{Edd}} = 1$ one can calculate the mass of the black hole I implicitly assumed by my model of the lightcurve. The model is really for super massive black holes with masses of $\approx 3.16 \times 10^8 M_{\odot}$. But not only tidal disruption events by super massive black holes are interesting. TDEs by intermediate mass black holes (IMBHs), where the exact mass range is still unknown, are even more interesting because the timescale, on which these objects have a declining flux, is much smaller. Additionally, IMBHs are thought to be not as rare as SMBHs and therefore the detection of TDEs by IMBHs should happen more often. To take the mass dependence of the lightcurve into account, I implemented the formula given by equation 3.18. The flux in the quiescent phase I set to 0. The flux corresponding to L_0 is the flux that is listed in table 6.1. Now I could change the black hole mass and investigate tidal disruption events by intermediate mass black holes.

This means I have a source catalogue with fixed black hole mass of $\approx 3.16 \times 10^8 M_{\odot}$, where the lightcurve is given by equation 6.2 and I have a source catalogue with variable black hole mass, where the lightcurve is more complicated and given by equation 3.18. Both source catalogues can be used as input files for simulations for *eROSITA*.

Fig. 6.1 shows a comparison between a lightcurve for a $3 \times 10^8 M_{\odot}$ black hole (left) and for a $10^3 M_{\odot}$ black hole (right), respectively, as they can be found in the simput-file. One can easily see that the timescale with flux unequal to 0 becomes very short for an intermediate mass black hole in comparison to a super massive black hole. Therefore, it is already at this point apparent that *eROSITA* has to catch a tidal disruption event by a IMBH right at its sudden rise or only shortly after. Otherwise it is in its quiescent state again.

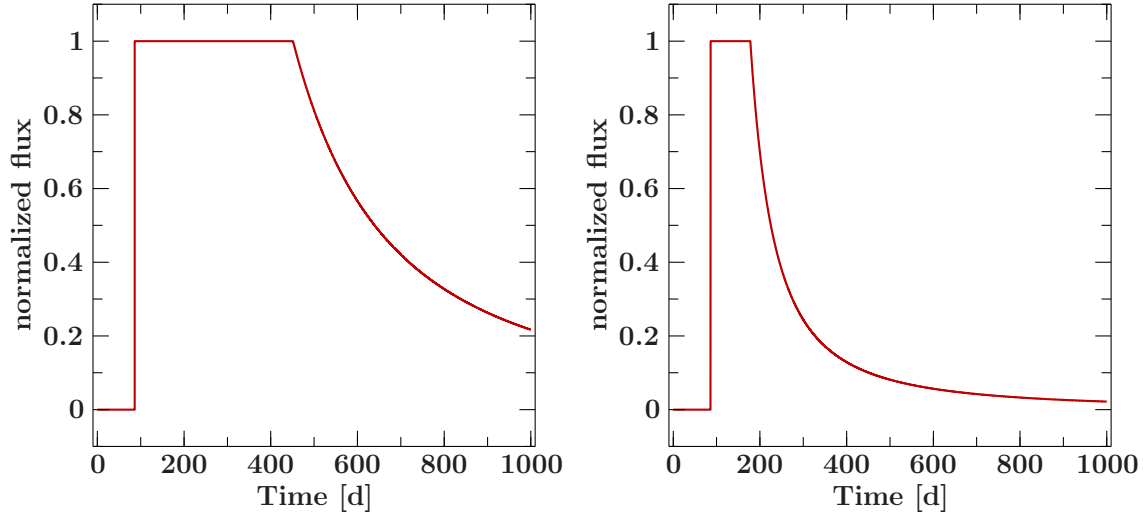


Figure 6.1: Lightcurve of a $3 \times 10^8 M_{\odot}$ (left) and a $10^3 M_{\odot}$ (right) mass black hole as it is in the simput-file.

6.2 Result of the all-sky survey simulation

For simplicity I concentrated on NGC 5905, which is with a flux of $2.61 \times 10^{-11} \text{ erg s}^{-1} \text{ cm}^2$ in the 0.1 – 10 keV band a quite luminous source. I chose this source because of its brightness and because it was accidentally the first one in the source catalogue. In order to not have to simulate a whole 6-month all-sky survey I at first searched when *eROSITA* will be scanning the coordinates of that source. Therefore, I used the attitude file and looked up when the coordinates of NGC 5905 (which I chose randomly) ± 20 arcmin are in the field of view of *eROSITA*. Only this time span of the all-sky survey I simulated. Additionally I switched the background off to see only the behavior of the source. Six consecutive revolutions (i.e., 24 h) were written into a single event file. The resulting seven event files (one for each detector) were merged together to one final event file. With the help of the `fselect` command I cut out a box of both height and width 20 arcmin, centered on the source coordinates. I used this final, selected file for my analysis.

My aim is to investigate if it is possible to classify a luminous flare as a tidal disruption event already within one six month series of passages. To investigate this possibility, I simulated a “normal” TDE with decaying flux, and also a source with constant flux equal to the peak flux of the “normal” TDE. A comparison of both would show whether the decrease in flux is significant enough to be measured to high confidence or not. Therefore I used the ISIS function `lc_from_events` to get a lightcurve out of the event files that resulted from the simulation. With the help of `merge_struct_arrays` I merged the lightcurves from all event files which contain the source. This merged lightcurve I filtered with `struct_filter` to know at which times I really have a signal. After that I split the resulting lightcurve in blocks separated by gaps with no signal for at least one hour. This is done with the help of `split_lc_at_gaps`. Within these blocks I afterwards summed all counts and took the average of the time. The error in counts is calculated as the square root of the counts. This can now be plotted and a comparison between constant flux and decaying flux can be made.

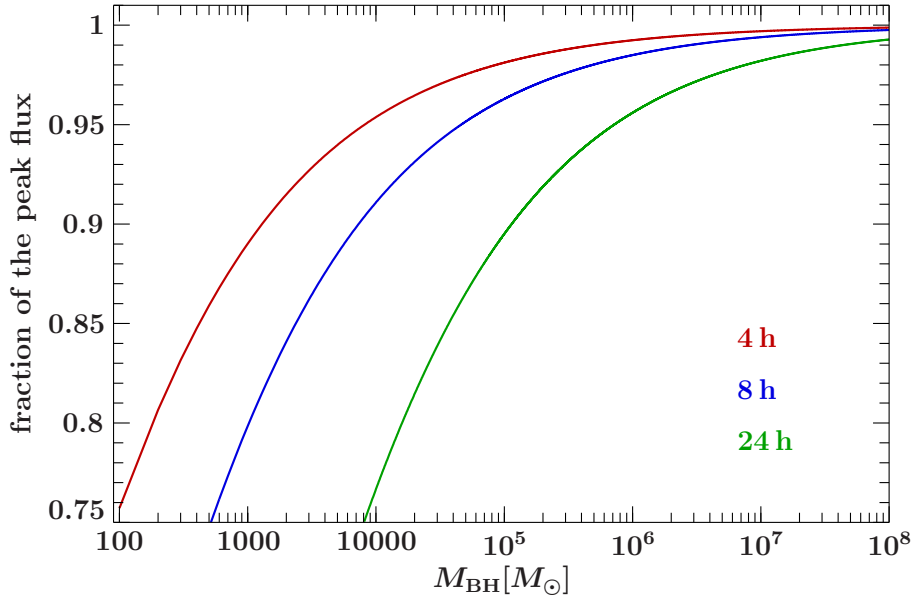


Figure 6.2: Mass dependence of the decay in flux. The red line denotes the flux after 4 h, the blue line after 8 h, and the green line after 24 h for different black hole masses.

Fig. 6.2 shows how fast the flux of a source drops for different black hole masses. It is apparent that the flux of a super massive black hole with $M_{\text{BH}} > 10^6 M_{\odot}$ drops only a few percent, even after 24 h. In contrast, the decrease for intermediate mass black holes is much more rapid. Already after 4 h the flux of a $10^3 M_{\odot}$ black hole is almost 10 percent lower than before. 24 h after the disruption it reaches even less than 30 percent of the original peak flux, which is rather faint.

6.2.1 Results for TDEs by SMBHs

In this subsection I use the first approach of modelling the lightcurve without black hole mass dependence. Therefore, all calculations and simulations here refer to a SMBH with a mass of $\approx 3 \times 10^8 M_{\odot}$.

Fig. 6.3 shows the count rate over time. One can see how the source slowly moves into *eROSITA*'s field of view and then out of it again. This phenomenon corresponds namely to an increase and a decrease in count rate, respectively. Statistical deviations cause some minor drops but the overall shape is first an increase in flux till a peak is reached when the source is right in the middle of *eROSITA*'s field of view. Afterwards the flux decreases again. Fig. 6.4 shows a zoom into one passage. It is clearly visible how the source moves into *eROSITA*'s field of view and out of it again.

In Fig. 6.5 this effect can be seen as well. Here the summed counts of each block are plotted over the averaged time in each block. The increase and decrease in flux are both quite apparent. Blue denotes here a source with constant flux and red one with a $t^{-5/3}$ decay. As one can see only little difference is recognizable. This means that it is very unlikely up to impossible to classify a luminous flare as a tidal disruption event within one day, at least if it is a super massive black hole.

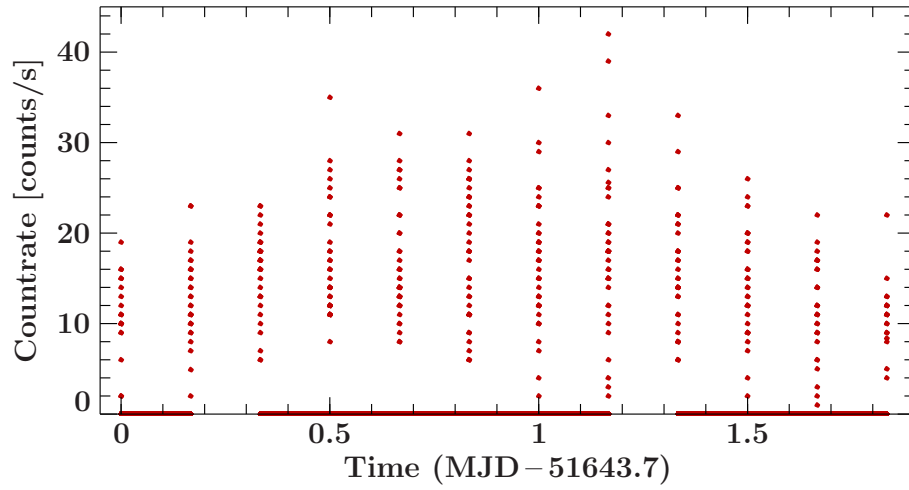


Figure 6.3: Count rate over time for a SMBH. As the source slowly gets into *eROSITA*'s field of view the count rate first increases with time. Then the source moves out of *eROSITA*'s field of view again and the count rate decreases.

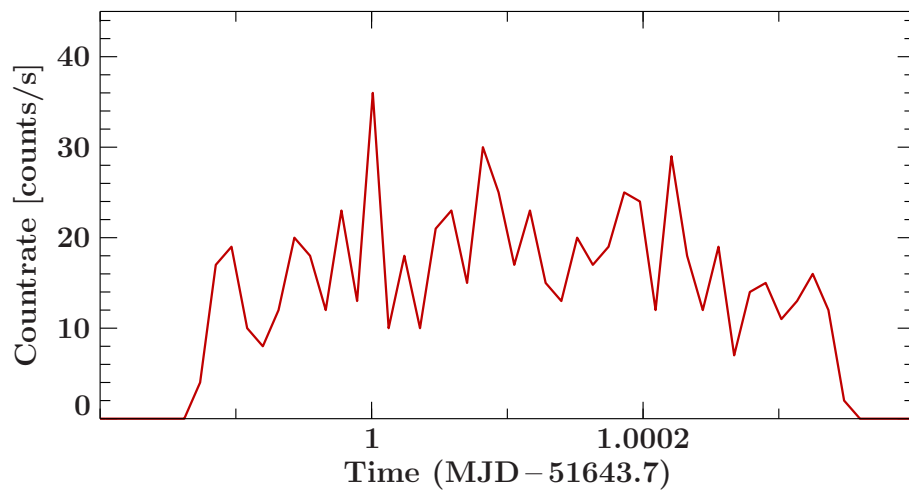


Figure 6.4: Zoom into one passage. The increase and decrease in flux is clearly visible as the source moves into and out of *eROSITA*'s field of view.

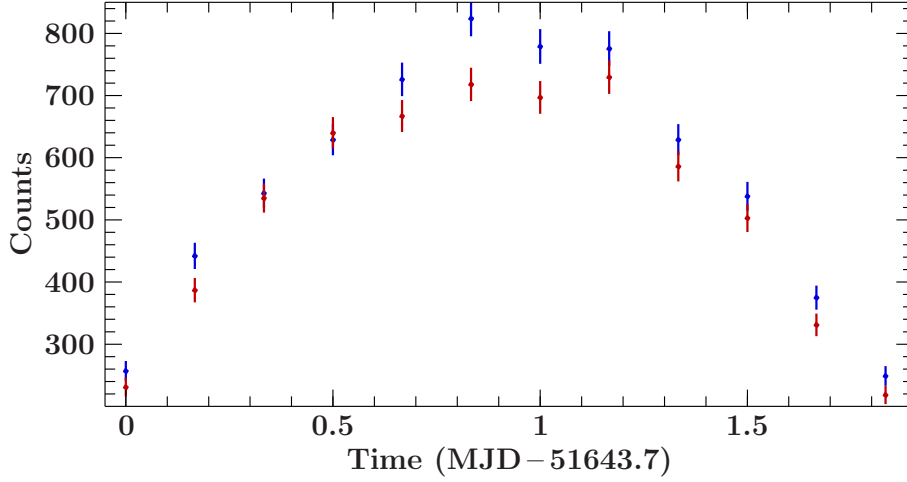


Figure 6.5: Summed counts in each block plotted over time for a SMBH. Red denotes the summed counts for a $t^{-5/3}$ decay, blue the ones for a constant flux over time. Note that there is only a little difference between both.

To verify this result by theoretical calculations, one has to estimate the drop in flux. NGC 5905 is right in the middle of *eROSITA*'s field of view about 14.5 days after the decay in flux starts. Therefore, the drop in flux after 4 h can be calculated as follows:

$$\frac{F_2}{F_1} = \left(\frac{14.666 \text{ d}}{14.5 \text{ d}} \right)^{-5/3} = 0.9812 \quad (6.3)$$

Assuming now a maximum number of counts of 700, for a 3σ -detection a drop in flux of at least $3\sqrt{700} \approx 3 \cdot 26.5 = 79.5$ counts is needed. A decline of about 1.88% corresponds to 13.16 counts, which means it would only be a 0.17σ -detection and therefore is not significant enough to classify it for sure as was already stated above.

It would be interesting to know whether a higher luminosity would allow a 3σ -detection and how many times higher it should be therefor. To investigate these questions, I simulated a 100 times brighter source and analyzed it as described above. The result can be found in panel a) of Fig. 6.6. A decline in flux of 1.88% corresponds here to about 573.4 counts assuming a maximum amount of 30500 counts. That means it would be a 3.28σ -detection, which is thought to be a real measured decay and not due to statistical fluctuations. But this is only because of the brightness of the source. If one looks at panel b) of Fig. 6.6, then it seems clear that one would not be able to distinguish a TDE by a super massive black hole from a source with constant flux since in panel b) of Fig. 6.6 the ratio between a normal decaying TDE and a source with constant flux is plotted. Additionally, the ratio was divided by its average to get fluctuations around 1. The error is about 1% and the fluctuations are only due to statistical effects. Therefore, it is not possible to distinguish both cases. The offset between the simulated decaying and the constant source results from the decline in flux. In the simulations the start of the decay is about 14.5 days before, which leads to a flux less than the peak flux. But I use the peak flux for the constant source. In this way an offset is produced between both sources.

To estimate now the brightness of a source needed to be detected with 3σ , one has to

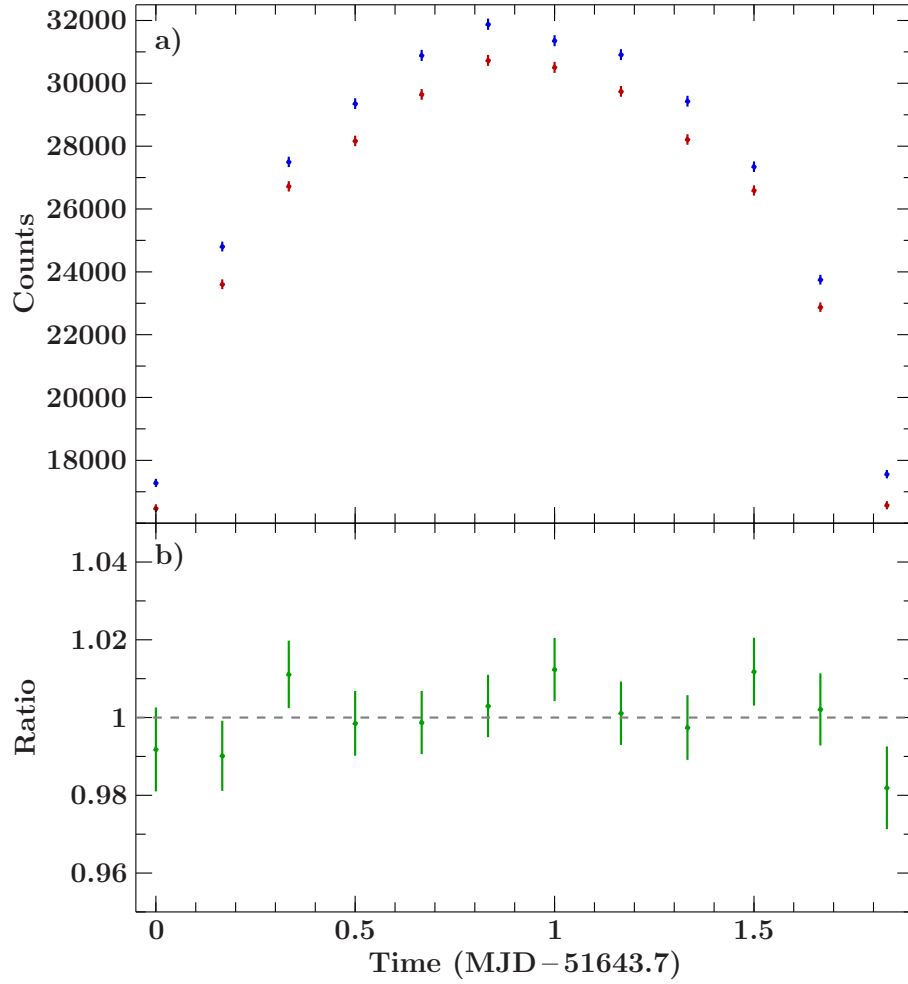


Figure 6.6: Panel a) shows the summed counts in each block plotted over time for a 100 times brighter SMBH than in Fig. 6.5. Red denotes the summed counts for a $t^{-5/3}$ decay, blue the ones for a constant flux over time. In panel b) the ratio of the summed counts of the normal decaying TDE to the one with constant flux in the case of a SMBH is plotted. The ratio is divided by its average to have fluctuations around 1.

solve the equation

$$3\sqrt{x} = 0.0188 \cdot x, \quad (6.4)$$

where x represents the unknown amount of maximum counts. Solving this equation above gives $x = 25.46 \times 10^3$. In order to get a rough approximation of the corresponding flux I assumed a linear proportionality between the flux and the number of counts. A 100 times brighter source corresponds to a 100 times higher amount of counts, at least theoretically. In the simulations the number of counts is only 43 times higher for a 100 times brighter source. This effect is caused by pileup. When two or more photons hit the same or adjacent pixel on the detector during one frame, it is possible that the created pattern is invalid as it is unknown how many photons of which energy hit the detector in which pixel. Because of this reason, the event is discarded. Further information on pileup and its impact on simulations for *eROSITA* can be found in Hain (2017). Due to pileup the resulting amount of counts is therefore reduced and I estimated

$$\frac{C_1}{700} = 0.43 \frac{F_1}{2.61 \times 10^{-11} \text{ erg s}^{-1} \text{ cm}^{-2}}, \quad (6.5)$$

where C_1 and F_1 represent the number of maximum counts and the flux, respectively, which are searched for. For $C_1 = 25.46 \times 10^3$ the flux is $F_1 = 2.21 \times 10^{-9} \text{ erg s}^{-1} \text{ cm}^{-2}$. This is the minimum flux a source should have to detect a decline in flux with a sufficient probability, at least in theory. But this minimum flux is no guarantee that it can be distinguished from a source with constant flux. Because the brighter the source is, the more counts correspond to a small decline in flux and the higher the σ -detection. Therefore, there is no evidence for a real decline in flux. In addition all the above calculations do not include background. If it would be included, it might add some more uncertainty, although it is constant. Additionally, I assumed that the source is seen by *eROSITA* about 14 days after the disruption. If the source would be detected in an earlier phase, the decline in flux should be higher and therefore the limiting flux for a 3σ -detection should be lower. For the case when the source is detected years after the disruption, the decline in flux should become much slower and a brighter source would be needed to detect a significant decay in flux. However, if the source was not very bright at its peak it maybe can not be detected at all after such a long decaying phase.

6.2.2 Results for TDEs by IMBHs

In principle the same that has been done for super massive black holes can be transferred to intermediate mass black holes. In Fig. 6.7 the count rate of an intermediate mass black hole with $10^3 M_\odot$ is shown. In the following I also use simulations for a BH with this mass. The overall shape of an increase and a decrease in flux can not be seen here as good as in contrast in Fig. 6.3. This effect is caused by the rapid decline of the flux. At the time, when the source gets into *eROSITA*'s field of view, the flux is constant. But at some point the decaying phase starts, while *eROSITA* is still seeing the source. As the decline is very rapid, the slow decay when the source moves out of *eROSITA*'s field of view can not be seen as good as for a SMBH.

There is still only few known about IMBHs. But one assumption is that there are more IMBHs than SMBHs. Therefore, tidal disruption events by intermediate mass black holes should happen more often than those by super massive black holes. As the field of view of

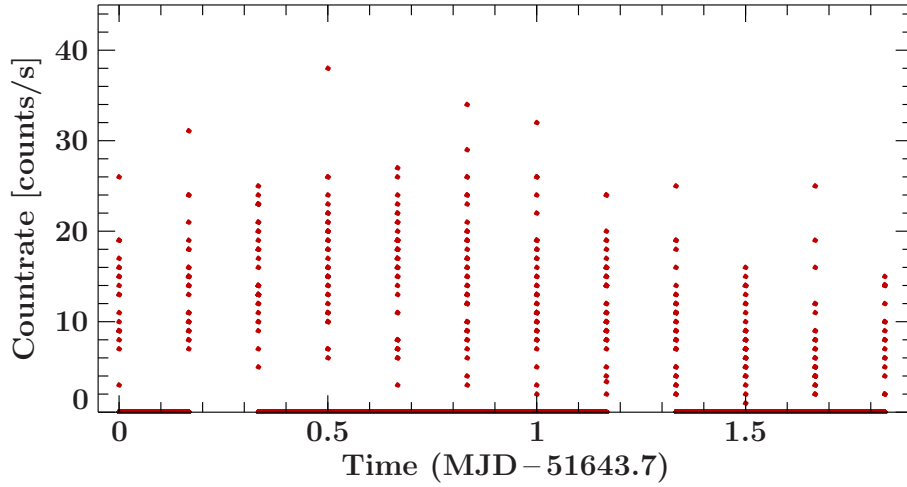


Figure 6.7: Count rate over time for a IMBH. As the source slowly gets into *eROSITA*'s field of view the count rate first increases with time. Then the source moves out of *eROSITA*'s field of view again and the count rate decreases. The decrease in count rate starts already before the source reaches the middle of *eROSITA*'s field of view because the decline in flux is so high.

telescopes is rather small, the probability to detect a TDE just by accident is very small. Additionally the decline in flux of a TDE by an IMBH is very rapid so that we can not easily detect one. Here *eROSITA* will be a game changer. As it is scanning the entire celestial sphere for four years, the probability to detect a TDE by an IMBH is lifted. That makes simulations of TDEs by IMBHs very interesting until the first real data taken by *eROSITA* are available.

In panel a) of Fig. 6.8 the effect of the fast decline in flux can even be better seen. As in panel a) of Fig. 6.6, blue denotes here the summed counts for a constant flux. Red shows how it looks when *eROSITA* detects the tidal disruption event in the phase of constant flux. For this reason it looks quite the same as blue. The few differences could result from statistical effects. Orange represents a detection shortly after the beginning of the declining phase. Therefore, the measured counts are already less at the beginning. And as the flux keeps decaying, the moving of the source into and out of *eROSITA*'s field of view can not be seen very good. Green shows kind of a mixture of orange and red. At first the source is seen in the phase of constant flux. But then the decay starts and strong deviations from the detection in the constant phase can be measured. The count rate for this case was shown in Fig. 6.7. It is quite obvious that, if *eROSITA* detects a tidal disruption event right at the border between constant phase and decaying phase, the luminous flare could be identified as a tidal disruption. If the source resides at the constant phase, it can not be distinguished from a source with constant flux and therefore would not be classified as a tidal disruption. At least not after one move through *eROSITA*'s field of view. But in the next all-sky survey six month later, the decline in flux compared to the value half a year before would be significant enough. If *eROSITA* detects a TDE in its decaying phase, it is not such obvious that it could be classified as one, too. Therefore, I created the same plot as in panel b) of Fig. 6.6, but this time for a IMBH. The result

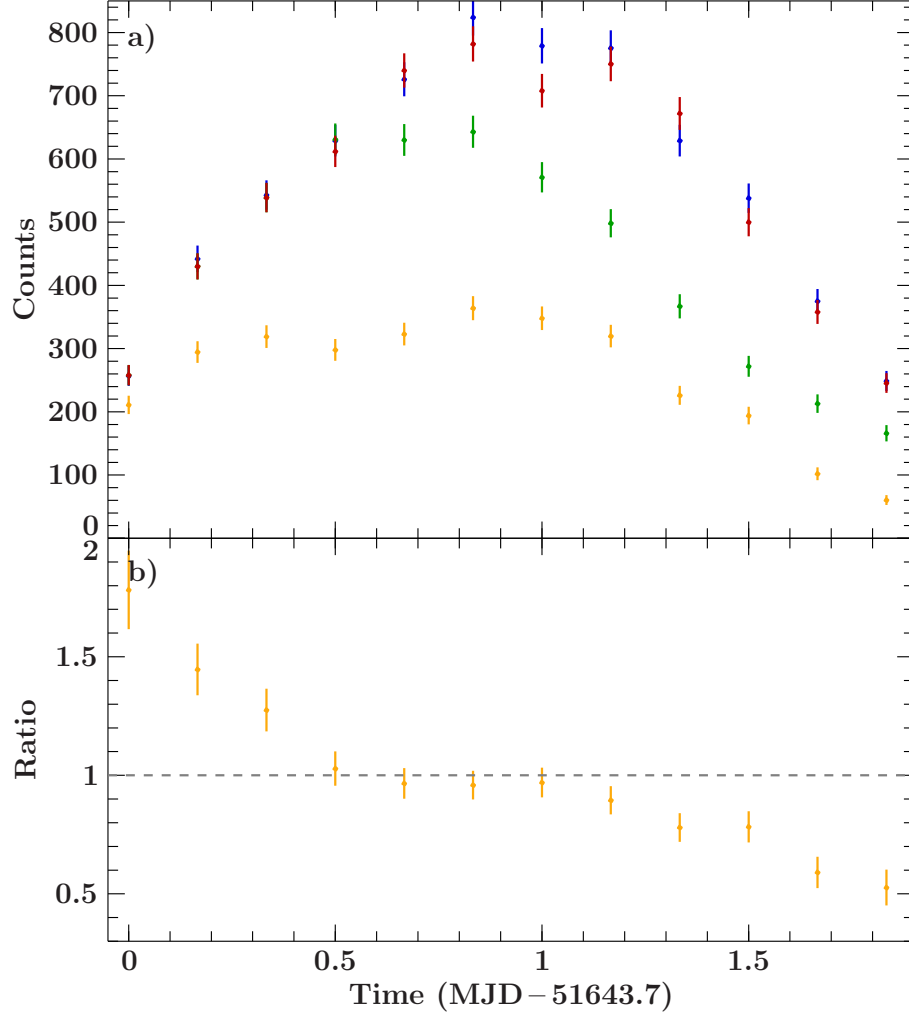


Figure 6.8: Panel a) shows the summed counts in each block plotted over time for an IMBH with mass $10^3 M_{\odot}$. Blue denotes the summed counts for a constant flux. The other points show how *eROSITA* sees a tidal disruption at different times after disruption. Red stands for a scan of *eROSITA* during the constant phase of the lightcurve, orange shortly after the beginning of the decaying phase, and green at both, the constant phase and the decaying phase as well. In panel b) the ratio of the summed counts of the normal decaying TDE (orange line in upper panel) to the one with constant flux in the case of an IMBH is plotted. The ratio is divided by its average to have fluctuations around 1.

can be found in panel b) of Fig. 6.8. In contrast to the case of a SMBH, this time the deviations are very obvious. The decline in flux can therefore be measured and maybe one could classify it as a tidal disruption event. Or at least, propose follow up observations to get a better understanding of the behavior of the source.

To confirm the intuitive conclusions by calculations, I used

$$\frac{F_2}{F_1} = \left(\frac{t + 4 \text{ h} - t_0}{\tau_{Edd}} \right)^{-5/3} \left(\frac{\tau_{Edd}}{t - t_0} \right)^{-5/3} = \left(\frac{t + 4 \text{ h} - t_0}{t - t_0} \right)^{-5/3}, \quad (6.6)$$

which follows from equation 3.18. Note that this relation is now independent of the black hole mass. As the source is right in the middle of *eROSITA*'s field of view about 1.4 days after the beginning of the declining phase the drop in flux is 17.39%. Assuming a maximal number of counts of 300, the drop in flux after 4 h would be detected with approximately 3.01σ .

6.3 Conclusions of the simulations

To summarize the results of the simulations, it is obvious that *eROSITA* will not be able to detect tidal disruption events by SMBHs by the decline in flux within only one scan of the sky. The second scan a half year later is needed to determine a decay in flux with a sufficient certainty.

For TDEs by IMBHs that is not the case. Here the decline in flux is rapid enough to be determined within few hours. If *eROSITA* catches the event right at the transition from constant flux to decaying flux, it can be identified as a tidal disruption event. Even if the source moves into *eROSITA*'s field of view few hours after the decline in flux has started, a change in flux can be measured. As TDEs by IMBHs should happen quite often, I expect *eROSITA* to detect many of them during its all-sky surveying phase.

7 Conclusions

To summarize what I found out in my thesis about TDE, I start with the data analysis part. Here I saw that the spectra of the both sources could be modelled well with an (absorbed) power law. A black body component does not improve the fits. Therefore, I can confirm the results of Cenko et al. (2012), who found an absorbed power law as the best fit for *Swift* J2058.4+0516. The result of Esquej et al. (2012) I can not confirm because they stated that a black body plus power law would describe the data best. But I found a pure power law being the best fit. Maybe the reason therefor is that Esquej et al. (2012) does not use a single spectrum but three, which were taken by different telescopes and at different times. Theory predicts a spectral hardening with time. Therefore, it can be possible that this hardening is the reason for the differing best fit models as I only used one spectrum for my analysis.

After the analysis I had a rough idea how a spectrum of a TDE looks like. Then I wanted to know whether a tidal disruption event could be detected by an all-sky survey. Or especially, if the drop in flux, which is predicted by theory, can be measured within a short period of time. *eROSITA* will be doing the next all-sky survey in the X-ray band. Therefore, I did all simulations for this instrument. At first I had to create a source catalogue of different known TDEs to use it as input for the simulations. I concentrated on one single source, that I chose quite randomly. Additionally I only simulated the time when the source is in *eROSITA*'s field of view. I extracted a lightcurve out of the simulated event files. Then I split the lightcurves into blocks and summed the counts in these blocks. The summed counts plotted over time show how the source moves into *eROSITA*'s field of view and out of it again. Furthermore, I investigated if a source with a decay in flux as it is predicted by theory can be distinguished from a source with constant flux. My result was that for TDEs by SMBHs the decline is not significant enough to be detected within 4 h. Even with very bright sources it is not possible. Therefore, a TDE by a SMBH will probably not be classified as one until *eROSITA* moves a second time, half a year later, over the source. At this time follow-up observations are still interesting anyway. For example, the spectral hardening with time could be investigated further on.

Additionally I looked at a simulated TDE by a IMBH. Here the decay in flux can be seen very good after 4 h. Due to this fact a tidal disruption by a intermediate mass black hole will probably be detected well within 4 h. Though, the brightness of the source could be problematic. As the decay in flux is very rapid, a faint source could be too faint after a short period of time to still detect it. Furthermore, a TDE only will be recognized as one if it is detected at the border between constant phase and decaying phase or shortly after the beginning of the decline in flux. Otherwise, if it is detected a long time afterwards, the drop in flux is too high. Nevertheless, I expect *eROSITA* to detect many of them during its four years of all-sky survey.

8 Outlook

I did first simulations of how tidal disruptions events look like if they are detected by *eROSITA*. Therefore, there is still quite some work to do. For example, I chose the coordinates of the sources randomly. Further simulations could be done with a more realistic distribution of TDEs over the sky. The distribution also depends on the mass of the black hole. Additionally the right rates for TDEs should be used. Estimates of the expected rate for SMBHs can be found in Komossa (2015, and references therein). The estimates for TDEs by IMBHs are even higher. Also considering the distribution of IMBHs over the sky would be interesting. But there is not that much known about intermediate mass black holes to date.

Another improvement would be to consider the right luminosity of intermediate mass black holes. For simplicity I chose the same flux as for super massive black holes. Furthermore, the dependence of the black hole mass could be investigated in more detail. Therefore more simulations with different masses could be done and the results could be compared. One could also estimate the lower limiting mass of a black hole for detecting a tidal disruption event.

Further improvement of the predictions how *eROSITA* will see TDEs could be given by correcting the simulations for the PSF and other effects caused by systematic effects. Furthermore, the eSASS software could be used to extract lightcurves. This software was developed for extracting data simulated for *eROSITA*.

What could be done as well is to study the change in spectrum over time. I think this can only be done with real data taken by *eROSITA*. Because as far as I know it is still unknown how exactly the spectrum of a TDE changes with time.

But I think if the suggestions above are included in further work, then we will have a good picture of how *eROSITA* will see TDEs and the identification of tidal disruption events will be alleviated. Additionally in the first real data taken by *eROSITA* we will find hopefully quite a big number of TDEs so that we can understand this interesting sort of X-ray emitting sources better and improve our knowledge about it when there are much more events known than today.

References

- Bade N., Komossa S., Dahlem M., 1996, *Astronomy and Astrophysics* 309, L35
- Barthelmy S.D., Barbier L.M., Cummings J.R., et al., 2005, *Space Science Reviews* 120, 143
- Cappelluti N., Ajello M., Rebusco P., et al., 2009, *Astronomy and Astrophysics* 495, L9
- Cenko S.B., Krimm H.A., Horesh A., et al., 2012, *ApJ* 753, 77
- Chen X., Madau P., Sesana A., Liu F.K., 2009, *ApJ* 697, L149
- Esquej P., Saxton R.D., Freyberg M.J., et al., 2007, *ApJ* 462, L49
- Esquej P., Saxton R.D., Komossa S., Read A.M., 2012, In: *European Physical Journal Web of Conferences*, Vol. 39. *European Physical Journal Web of Conferences*, p. 02004
- Esquej P., Saxton R.D., Komossa S., et al., 2008, *Astronomy and Astrophysics* 489, 543
- Evans C.R., Kochanek C.S., 1989, *ApJ* 346, L13
- Frank J., Rees M.J., 1976, *MNRAS* 176, 633
- Freitag M., Benz W., 2002, *Astronomy and Astrophysics* 394, 345
- Gezari S., Chornock R., Rest A., et al., 2012, *Nature* 485, 217
- Gezari S., Heckman T., Cenko S.B., et al., 2009, *ApJ* 698, 1367
- Gezari S., Martin D.C., Milliard B., et al., 2006, *ApJ* 653, L25
- Greiner J., Schwarz R., Zharikov S., Orio M., 2000, *Astronomy and Astrophysics* 362, L25
- Grupe D., Thomas H.C., Leighly K.M., 1999, *Astronomy and Astrophysics* 350, L31
- Guillochon J., Manukian H., Ramirez-Ruiz E., 2014, *ApJ* 783, 23
- Guillochon J., Ramirez-Ruiz E., 2013, *ApJ* 767, 25
- Hain T., 2017, *Master's thesis*, Friedrich-Alexander-Universität Erlangen-Nürnberg
- Hanisch R.J., Farris A., Greisen E.W., et al., 2001, *Astronomy and Astrophysics* 376, 359
- Hills J.G., 1975, *Nature* 254, 295
- Kesden M., 2012, *Physical Review D* 85, 024037
- Khabibullin I., Sazonov S., Sunyaev R., 2014, *MNRAS* 437, 327
- Komossa S., 2012, In: *European Physical Journal Web of Conferences*, Vol. 39. *European Physical Journal Web of Conferences*, p. 02001
- Komossa S., 2015, *Journal of High Energy Astrophysics* 7, 148
- Komossa S., Greiner J., 1999, *Astronomy and Astrophysics* 349, L45
- Krauss F., 2016, Ph.D. thesis, Friedrich-Alexander-Universität Erlangen-Nürnberg
- Krimm H.A., Kennea J.A., Holland S.T., et al., 2011, *Astron. Tel.* 3384
- Lacy J.H., Townes C.H., Hollenbach D.J., 1982, *ApJ* 262, 120
- Lin D., Carrasco E.R., Grupe D., et al., 2011, *ApJ* 738, 52
- Lin D., Maksym P.W., Irwin J.A., et al., 2015, *ApJ* 811, 43
- Lodato G., Franchini A., Bonnerot C., Rossi E.M., 2015, *Journal of High Energy Astrophysics* 7, 158
- Lodato G., King A.R., Pringle J.E., 2009, *MNRAS* 392, 332
- Maksym W.P., Lin D., Irwin J.A., 2014, *ApJ* 792, L29
- Maksym W.P., Ulmer M.P., Eracleous M., 2010, *ApJ* 722, 1035
- Maksym W.P., Ulmer M.P., Eracleous M.C., et al., 2013, *MNRAS* 435, 1904
- Meidinger N., Andritschke R., Elbs J., et al., 2011, In: *Society of Photo-Optical Instrumentation Engineers (SPIE) Conference Series*, Vol. 8145. *Proceedings of the SPIE*, p. 814502
- Merloni A., Predehl P., Becker W., et al., 2012, *ArXiv e-prints*
- Pavlinisky M., Sunyaev R., Churazov E., et al., 2008, In: *Space Telescopes and Instrumentation 2008: Ultraviolet to Gamma Ray*, Vol. 7011. *Proceedings of the SPIE*, p. 70110H
- Pehle T., Waschi H.P., (eds.) 2011, *Formelsammlung Naturwissenschaften*, Cornelsen-Verlag
- Pence W.D., Chiappetti L., Page C.G., et al.,

- 2010, *Astronomy and Astrophysics* 524, A42
- Phinney E.S., 1989, In: Morris M. (ed.) *The Center of the Galaxy*, Vol. 136. IAU Symposium, p. 543
- Predehl P., 1999, In: Siegmund O.H., Flanagan K.A. (eds.) *EUV, X-Ray, and Gamma-Ray Instrumentation for Astronomy X*, Vol. 3765. *Proceedings of the SPIE*, p.172
- Predehl P., 2012, In: *Space Telescopes and Instrumentation 2012: Ultraviolet to Gamma Ray*, Vol. 8443. *Proceedings of the SPIE*, p. 84431R
- Predehl P., Andritschke R., Babyshkin V., et al., 2016, In: *Space Telescopes and Instrumentation 2016: Ultraviolet to Gamma Ray*, Vol. 9905. *Proceedings of the SPIE*, p. 99051K
- Predehl P., Andritschke R., Böhringer H., et al., 2010, In: *Space Telescopes and Instrumentation 2010: Ultraviolet to Gamma Ray*, Vol. 7732. *Proceedings of the SPIE*, p. 77320U
- Predehl P., Andritschke R., Bornemann W., et al., 2007, In: *UV, X-Ray, and Gamma-Ray Space Instrumentation for Astronomy XV*, Vol. 6686. *Proceedings of the SPIE*, p. 668617
- Predehl P., Friedrich P., Hasinger G., et al., 2003, *Astronomische Nachrichten* 324, 128
- Predehl P., Hasinger G., Böhringer H., et al., 2006, In: *Society of Photo-Optical Instrumentation Engineers (SPIE) Conference Series*, Vol. 6266. *Proceedings of the SPIE*, p. 62660P
- Rees M.J., 1988, *Nature* 333, 523
- Rees M.J., 1989, In: Klare G. (ed.) *Reviews in Modern Astronomy*, Vol. 2. *Reviews in Modern Astronomy*, p.1
- Sari R., Kobayashi S., Rossi E.M., 2010, *ApJ* 708, 605
- Saxton R.D., Motta S.E., Komossa S., Read A.M., 2015, *MNRAS* 454, 2798
- Saxton R.D., Read A.M., Esquej P., et al., 2012a, *Astronomy and Astrophysics* 541, A106
- Saxton R.D., Read A.M., Komossa S., Esquej P., 2012b, In: *European Physical Journal Web of Conferences*, Vol. 39. *European Physical Journal Web of Conferences*, p. 02002
- Schmid C., 2012, Ph.D. thesis, Friedrich-Alexander-Universität Erlangen-Nürnberg
- Stone N., Sari R., Loeb A., 2013, *MNRAS* 435, 1809
- Strubbe L.E., Quataert E., 2009, *MNRAS* 400, 2070
- Truemper J., 1982, *Advances in Space Research* 2, 241
- Wilms J., Allen A., McCray R., 2000, *ApJ* 542, 914
- Wolter H., 1952a, *Annalen der Physik* 445, 94
- Wolter H., 1952b, *Annalen der Physik* 445, 286

Acknowledgment

At the end of this thesis I want to thank all the people that helped me during my work. Thanks to my supervisor Jörn Wilms who let me work on this interesting topic. Special thanks to Thomas Dauser for his help with ISIS and SIXTE. I hope I did not annoy you with all my (stupid) questions. Second special thanks to Philipp Weber who started working on simulations for *eROSITA* with me and who helped me with all my little and big problems with programming when Thomas was not around. But it seems to me as if I have asked all of the people here at the observatory for help every now and then. Big thanks to all of you! Thank you for helping me solving my problems, but also for all the fun and cake (of course)! I really enjoyed the atmosphere at the observatory!

I do not want to thank only the people at the observatory but also my friends and family. Thanks to my friends from school who see me only occasionally, but are always interested in what I am doing although their idea of what I am doing does not fit with reality. Most of the time I do not look at the sky but at my computer. Nevertheless, a big thanks to you for introducing me to real life. Thanks to my friends here in Erlangen. For funny conversations during train rides, for lamenting together and all the fun we had together. Big thanks to my boyfriend and his family. He is always there when I need him and still endures me, surprisingly. Additionally he makes me relax even in the most stressful times. Last but not least a big thanks to my family. For their support and that my key still fit in the rare cases I could visit my parents. And of course for making me explain my topic in simple words and ask questions of which I had not thought before, which forced me to think about it and to understand it myself to express the answer in simple words. A big thank you for everything you did for me!

Eigenständigkeitserklärung

Hiermit bestätige ich, dass ich diese Arbeit selbstständig und nur unter Verwendung der angegebenen Hilfsmittel angefertigt habe.

(Ort, Datum)

Melanie Lang